Single-cell profiling uncovers regulatory programs of pathogenic Th2 cells in allergic asthma

Matarr Khan[1], Marlis Alteneder[1], Wolfgang Reiter[2,3], Thomas Krausgruber[4,5], Lina Dobnikar[4], Moritz Madern[1], Monika Waldherr[1], Christoph Bock[4,5], Markus Hartl[2,3], Wilfried Ellmeier[1], Johan Henriksson[6], and Nicole Boucheron[1*]

[1] Medical University of Vienna, Institute of Immunology, Division of Immunobiology, Center for Pathophysiology, Infectiology and Immunology, Vienna, Austria
[2] University of Vienna, Vienna Biocenter Campus (VBC), Department of Biochemistry and Cell Biology, Max Perutz Labs, Vienna, Austria
[3] University of Vienna, Vienna Biocenter Campus (VBC), Mass Spectrometry Facility, Max Perutz Labs, Vienna, Austria
[4]CeMM Research Center for Molecular Medicine of the Austrian Academy of Sciences, Vienna, Austria
[5]Medical University of Vienna, Institute of Artificial Intelligence, Center for Medical Data Science, Vienna, Austria
[6] Umeå University, the Laboratory for Molecular Infection Medicine Sweden (MIMS), Umeå Centre for Microbial Research (UCMR), Integrated Science Lab (Icelab), Department of Molecular biology, Umeå, Sweden

*Correspondence should be addressed to N.B. (nicole.boucheron@meduniwien.ac.at)

Abstract

Lung pathogenic T helper type 2 (pTh2) cells are important drivers of allergic asthma, but fundamental questions remain regarding their regulation and heterogeneity. The differentiation and effector functions of immune cells are tightly regulated by epigenetic processes. Histone deacetylase 1 (HDAC1) is an important epigenetic regulator of T cells, however, its role in pTh2 cells is yet to be determined. Here we investigate immune regulation in allergic asthma by single-cell RNA sequencing (scRNA-seq) in mice challenged with house dust mite, in the presence and absence of HDAC1 function. Our analyses reveal two distinct subsets of lung pTh2 cells: pathogenic effector Th2 (peTh2) and pathogenic Th2 tissue-resident memory (Th2 Trm) cells. Both pTh2 cell subsets are highly proinflammatory and exhibit distinct transcriptional and phenotypic signatures as compared with other lung Th subsets. Based on our scRNA-seq analysis, we identify conditions to generate pTh2 cells *in vitro* and confirm that these *in vitro* generated pTh2 cells have a similar transcriptional profile as lung peTh2 cells. Using our new *in vitro* model, we demonstrate that the p38 mitogen-activated protein kinase pathway is critical for interleukin-5 (IL-5) and IL-13 expression in pTh2 cells. Our data further underline the importance of HDAC1 in limiting the pathogenicity of lung and *in vitro* pTh2 cells and in the formation of lung Th2 Trm cells. In summary, we have generated novel insights into pTh2 cell biology and established a new *in vitro* model for investigating pTh2 cells that will be useful for discovering molecular mechanisms involved in pTh2-mediated allergic asthma.

Introduction

Asthma is a chronic lung disease affecting at least 300 million people worldwide and is among the most common non-communicable diseases globally[1, 2, 3]. It is characterised by increased airway inflammation, bronchial hyperresponsiveness, and airway remodelling; leading to shortness of breath, chest tightness, and wheezing[1]. Allergic asthma, the most frequent form of asthma in children and adults[1, 2, 4], is orchestrated by type 2 cytokine-producing cells such as type 2 innate lymphoid cells and T helper type 2 (Th2) cells along with epithelial-derived cytokines[1]. Upon allergen exposure, airway epithelial cells release a plethora of molecules including proinflammatory cytokines and alarmins[5, 6]. The latter include Interleukin-25 (IL-25), IL-33, and thymic stromal lymphopoietin (TSLP)[7], which in concert with antigen-presenting cells such as dendritic cells, promote the differentiation of Th2 cells from naïve $CD4^+$ T cells resulting in the secretion of type 2 cytokines, including IL-4, IL-5, IL-9, and IL-13, that drive disease progression[8].

Studies in humans and mice have identified a new Th2 cell subset termed pathogenic Th2 (pTh2) cells as the major inducers of allergic inflammation due to their propensity to secrete high levels of the type 2 cytokines IL-13 and particularly IL-5 (refs.[9, 10, 11, 12, 13, 14, 15, 16, 17, 18]). Due to their proallergic phenotype, pTh2 cells have become an important drug target not only in allergic asthma but also in other allergic diseases including allergic rhinitis, atopic dermatitis, eosinophilic esophagitis, and food allergy[12, 19, 20, 21, 22]. Despite the central role of pTh2 cells in allergic asthma, the cellular and molecular processes important for their differentiation and effector function have not been fully dissected[23, 24, 25]. A major obstacle to our understanding of pTh2 cell regulation is the lack of an *in vitro* model allowing high-throughput molecular and functional characterisation, which could potentially pave the way for developing novel therapies targeting them in allergic diseases.

It is well established that the differentiation of naïve $CD4^+$ T cells into distinct effector T helper (Th) subsets is controlled by multiple factors such as the cytokine milieu and chromatin state of the cells[26]. The latter has a profound effect on the acquisition, stability, and function of Th subsets[27]. The chromatin state of a cell is regulated by various epigenetic mechanisms such as reversible lysine acetylation mediated by histone acetyltransferases and histone deacetylases (HDACs)[28, 29]. We and others have demonstrated critical roles for HDACs in T cell biology[30, 31, 32].

HDACs have garnered interest as potential therapeutic targets in allergic asthma[33, 34, 35]. More recently, natural HDAC inhibitors such as short-chain fatty acids (SCFAs) have been considered for potential therapeutics for allergic asthma due to their immunomodulatory properties, mainly by suppressing the enzymatic activity of HDACs[36, 37]. Although promising, dissecting the role of HDACs in allergic asthma and particularly on pTh2 cell differentiation is needed to understand whether suppressing the activity of HDACs either pharmacologically or with natural inhibitors might represent a novel therapeutic approach to limiting allergic asthma. We previously reported that the deletion of HDAC1, a member of the class I histone deacetylases[28, 29] in T cells potentiated ovalbumin-induced allergic asthma[38]. However, the role of HDAC1 in pTh2 cell differentiation and effector function in response to the most important indoor aeroallergen for humans, house dust mite (HDM), has not been defined.

Here, using IL-13 tdTomato reporter mice[39] along with a HDM airway inflammation model and single-cell RNA sequencing (scRNA-seq) of $CD4^+$ T cells from lungs of healthy and diseased WT and HDAC1-cKO mice, we resolve the regulation of murine lung pTh2 cells, including their heterogeneity and subset-specific gene signatures. We identify and validate the presence of two distinct subsets of lung pTh2 cells, which express a plethora of proinflammatory molecules including *Il4*, *Il5*, *Il13*, *Tnfsf11*, *Areg*, *Tgfb1*, *Calc*a, and *Furin,* and exhibit shared and distinct transcriptional signatures. We observe some overlap between the pTh2 cell subsets and other lung $ST2^+$ Th cells and based on our data, establish a flow cytometry strategy to distinguish them. From our scRNA-seq analysis, we identify conditions that promote the generation of pTh2 *in vitro* thus resolving a major obstacle in allergy research. Our data establish a critical role for HDAC1 in regulating the differentiation and pathogenicity

of lung and *in vitro* generated pTh2 cells. Overall, our findings delineate the heterogeneity and signatures of pTh2 cells and generate novel insights into their molecular regulation.

Results

HDAC1 is essential to restrict HDM-induced airway inflammation

We have previously reported that the ablation of HDAC1 in T cells enhanced ovalbumin-induced allergic asthma[38]. But the role of HDAC1 in response to house dust mite (HDM), an environmental allergen, is unknown. To determine the impact of HDAC1 deletion in HDM-induced allergic asthma, we sensitised and challenged wild type (WT) and HDAC1 conditional knockout (HDAC1-cKO) mice with HDM (Extended Data Fig. 1a). Our analyses revealed an increased influx of eosinophils ($SiglecF^+CD11c^-$ cells) (Extended Data Fig. 1b-d) and total cellular infiltration (Extended Data Fig. 1e) in the bronchoalveolar lavage (BAL) of HDAC1-cKO mice, indicative of enhanced airway inflammation. To assess the role of HDAC1 in pathogenic type 2 cytokine expression by lung T helper (Th) cells, we isolated lung cells from PBS and HDM-exposed mice and restimulated them with PMA and ionomycin. Loss of HDAC1 augmented IL-5 and IL-13 expression in the *ex vivo* restimulated Th cells (Extended Data Fig. 1f, g). These results highlight the importance of HDAC1 in restricting HDM-induced airway inflammation and as a potential regulator of pTh2 cell differentiation.

scRNA-seq analysis of lung $CD4^+$ T cells uncovers the heterogeneity of pTh2 cells in response to HDM

Studies have identified pTh2 cells as the main drivers of allergic inflammation[9, 10, 11, 12, 13, 14, 15, 16, 17, 18], however, our understanding of the heterogeneity, signatures, and regulation of pTh2 cells is incomplete. To profile lung pTh2 cells and to dissect the role of HDAC1 in these cells, we used IL-13 tdTomato-reporter mice to enable us to track all IL-13-producing ($IL\text{-}13^+$) Th cells in response to HDM, including pTh2 cells[18]. We isolated lung cells and sorted $IL\text{-}13^+$ Th cells, non-IL-13 producing ($IL\text{-}13^-$) Th cells, and naïve $CD4^+$ T cells (naïve) from the lungs of WT and HDAC1-cKO mice exposed to PBS or HDM (as in Extended Fig. 1a). We obtained a total of ten samples based on the two genotypes (WT and HDAC1-cKO) and experimental conditions (PBS and HDM) (Fig. 1a).

After quality control, integration, and unsupervised clustering of our data, we identified fourteen distinct clusters (Extended Data Fig. 2a). We used a combination of known receptors, transcription factors (TFs), and cytokines to annotate the clusters (Extended Data Fig. 2b-d). Clusters 9, 10, 11, 12, and 13 were excluded from subsequent analyses due to cells of non-Th cell origin (clusters 11 and 13) or a small number of cells (Extended Data Fig. 2b and Supplementary Table 1). Our single-cell analysis revealed the presence of different $CD4^+$ T cell populations in the lung (Fig. 1b). Cells in clusters 0, 1, and 7 originated from naïve cells and expressed *Klf2*, *Ccr7*, and *Sell* (CD62L). Clusters 0 and 1 differed mostly in the expression of some ribosomal genes, while cells in cluster 7 showed upregulation of an interferon signature. Cells in cluster 3 represent activated cells with enhanced expression of *Cxcr3*, *Trat*1, *S1pr1*. Cells in clusters 4 and 8 expressed signatures of Th17 (*Il17a*, *Ccr6*, and *Rorc*) and Th1 (*Ccl5, Cxcr3*, and *Tbx21*) cells, respectively (Fig. 1c, Extended Data Fig. 3 and Supplementary Table 2).

Interestingly, both clusters 2 and 5 contained cells expressing pTh2 genes *Il4*, *Il5*, and *Il13* and additionally expressed high levels of *Il10*, *Areg*, *Tnfsf11*, *Calca,* and *Furin*. Distinguishing clusters 2 and 5 are the expression levels of pathogenic type 2 molecules and the tissue retention marker, *Cd69*. Cells in cluster 2, which we termed pathogenic effector Th2 (peTh2) cells, expressed higher levels of *Il4*, *Il5*, and *Il13*, while cells in cluster 5 showed enhanced expression of *Cd69* (Fig. 1c, Extended Data Fig. 3 and Supplementary Table 2). We named the cells in cluster 5 as Th2 tissue-resident memory (Th2 Trm) cells owing to their high mRNA expression of *Cd69*, a marker gene for Trm cells[40]. Moreover, previous studies have demonstrated that Th2 Trm cells emerge in the lungs of mice within a week

following allergen exposure, and persist for months[41, 42], thus supporting our classification of cells in cluster 5 as Th2 Trm cells.

Next, we performed gene set enrichment analysis (GSEA) to determine the similarity of the pTh2 cell subsets we have identified with recently reported airway pTh2 cells[18]. We used the peTh2 and Th2 Trm gene sets (Supplementary Table 2) and compared them with the recently published airway pTh2 gene set[18]. We found that both the peTh2 (Fig. 1d) and Th2 Trm (Fig. 1e) cell subsets were highly enriched for genes from the published gene set. The previous study did not further investigate whether the airway pTh2 cells contained distinct pTh2 cell subsets, however, our analysis indicates a strong overlap between these cells and the peTh2 and Th2 Trm cell subsets from this study (Fig. 1d-f and Supplementary Table 3), indicating that the published gene set might contain gene signatures belonging to both peTh2 and Th2 Trm cells. These observations highlight the strength of our approach of using IL-13 reporter mice, as it enables us to identify distinct pTh2 cell subsets (that is, peTh2 and Th2 Trm cells) and define their signatures.

Our analysis further uncovered a unique Th subset consisting of both Treg and Th2 signatures (cluster 6), thus we named cells in this cluster as Treg/Th2 cells (Fig. 1b, c and Extended Data Fig. 3). The signature of these Treg/Th2 cells included enhanced expression of *Il1rl1*, *Gata3*, *Bhlhe40*, *Areg*, *Gzmb*, and *FoxP3*, many of which are also enriched in peTh2 and Th2 Trm cells (Fig. 1c and 1g). Furthermore, in contrast to a previous report[43], we did not identify a distinct *Areg*-expressing pTh2 cell subset lacking *Il5*. Instead, we found co-expression of *Areg* and *Il5* by peTh2 cells (Fig. 1g). Collectively, our data resolve the heterogeneity of murine lung pTh2 cells, reveal their similarities with previously overlooked lung *Il1rl1*-expressing Th cells (Treg/Th2), and highlight the need to define markers to distinguish the pTh2 cell subsets from the Treg/Th2 subset.

Flow cytometric characterisation of lung pTh2 subsets in HDM-induced allergic asthma

Given some of the similarities we observed between the peTh2, Th2 Trm and Treg/Th2 subsets, particularly the expression of *Il1rl1* (Fig. 1g), it is important to define markers to distinguish them. This is crucial as ST2 is established as a marker to define pTh2 cells[15, 18, 42, 43, 44, 45]. Our analyses suggest that using ST2 alone is insufficient to define pTh2 cells since lung Treg/Th2 cells also expressed the gene. To this end, we used the DEGs in peTh2, Th2 Trm and Treg/Th2 (Supplementary Table 2) and compared them to identify surface markers that are distinctively expressed by these subsets. Our comparison revealed a remarkable overlap between these three subsets (Fig. 2a and Supplementary Table 3). However, we found that Treg/Th2 cells were enriched for *Klrg1* and *Cd27* as compared with the pTh2 cell subsets (Fig. 2a, b). To validate our observation, we performed a flow cytometric analysis of lung $CD4^+$ T cells from mice exposed to PBS or HDM. By using KLRG1, CD27, and additional surface markers (Fig. 2c and Extended Data Fig. 4), we first validated the expression of ST2 on $KLRG1^+$ and $CD27^+$ Th subsets (Treg/Th2 cells) (Fig. 3a-c). Unexpectedly, we found IL-13 expression in some of the $ST2^+KLRG1^+$ and $ST2^+CD27^+$ Th cells (Fig. 3b, c). These cells also expressed Foxp3 and Gata3 (Fig. 3d, e).

Based on the above observations (Fig. 3a-e), we sought to establish a flow cytometry gating strategy to properly define lung pTh2 cells. We first used CD27 and KLRG1 to exclude the Treg/Th2 subset, and surprisingly, found additional heterogeneity within this Th population. Our flow cytometric analysis revealed three distinct populations of Treg/Th2 cells: (1) $ST2^+CD27^+KLRG1^-$, (2) $ST2^+CD27^+KLRG1^+$, (3) $ST2^+CD27^-KLRG1^+$ (Fig. 3f). These Treg/Th2 populations contained cells expressing FoxP3 and IL-13 (Fig. 3g). We collectively refer to these populations of Treg/Th2 cells as non-pTh2 $ST2^+$ Th cells due to their high FoxP3 expression. By excluding these non-pTh2 $ST2^+$ Th cells, the remaining population of $ST2^+CD27^-KLRG1^-$ cells was highly enriched in $IL\text{-}13^+$ Th cells with only residual FoxP3 expression (Fig. 3g), indicating that the typical pTh2 cells are within the $ST2^+CD27^-KLRG1^-$ population. Thus, using CD27 and KLRG1 as markers to exclude non-pTh2 $ST2^+$ Th cells (Fig. 3f and Extended Data Fig. 4), and gating the remaining cells based on CD69 and PD-1 as additional Trm

marker[40] (Fig. 3h), we revealed that lung peTh2 cells can be identified as ST2$^+$CD27$^-$KLRG1$^-$CD69^{low}PD1^{high} (Fig. 3i), and Th2 Trm cells as ST2$^+$CD27$^-$KLRG1$^-$CD69^{high}PD1^{high} (Fig. 3k). We confirmed that these cells are indeed pTh2 cells due to their high IL-13 protein expression (Fig. 3j, l). Consistently, human allergen-specific pTh2 (Th2A) cells also exhibit a reduced level of CD27 (refs.[12, 46, 47, 48]). These findings support our strategy to use CD27, together with KLRG1, as key markers to exclude non-pTh2 ST2$^+$ Th cells. Overall, we have validated the presence of distinct lung ST2$^+$ Th subsets and defined surface markers to comprehensively distinguish them from the pTh2 cell subsets. Most importantly, we anticipate that using the surface markers we have proposed (Fig. 3m), lung pTh2 cell subsets can independently be isolated for further investigation.

Loss of HDAC1 augments the pathogenicity of pTh2 subsets and Th2 Trm cell generation

To determine the contribution of HDAC1 in the differentiation and effector function of lung pTh2 cell subsets, we grouped the cells by their origin (based on HTO labelling) (Fig. 4a, right). As expected, the majority (more than 80%) of cells in the two pTh2 cell clusters were IL-13$^+$ Th cells from mice exposed to HDM (Fig. 4a, right, and Supplementary Table 1). Notably, despite the low expression of *Il13* mRNA in the Th2 Trm cell subset (Extended Data Fig. 3), these cells expressed IL-13 protein (Fig. 4b and Supplementary Table 1). Additionally, we found that about 35% of cells in the Treg/Th2 cluster composed of IL-13$^+$ Th cells (Supplementary Table 1). This is in line with our flow cytometric analysis that some of the non-pTh2 ST2$^+$ Th cells expressed IL-13 (Fig. 3a-e). These results further strengthen our strategy to exclude non-pTh2 ST2$^+$ Th cells from the typical pTh2 cell subsets. Furthermore, we observed differences in the distribution of IL-13$^+$ Th cells from WT and HDAC1-cKO mice exposed to HDM in the peTh2 (cluster 2) (Fig. 4b, top) and Th2 Trm (cluster 5) (Fig. 4b, bottom) cell subsets. Most of the IL-13$^+$ Th cells in the peTh2 cell subset were from WT mice, while the Th2 Trm cell subsets consisted of more IL-13$^+$ Th cells from HDAC1-cKO mice (Fig. 4b and Supplementary Table 1). These observations suggest distinct differentiation stages between the two pTh2 cell subsets and a potential role for HDAC1 in regulating the processes involved. Further analysis of selected effector molecules and TFs expressed by the pTh2 cell subsets (Fig. 4c, d) revealed that HDAC1 is essential to restrict the expression of *Il5* and *Tnfsf11 (Rankl)* in the peTh2 cell subset (Fig. 4c).

An important aspect of allergic asthma is the generation of long-lived allergen-specific Th2 Trm cells that rapidly respond upon allergen re-exposure to orchestrate type 2 immune responses in the lung[15, 41, 42, 44, 45, 49, 50]. CD4$^+$ Trm cells are defined by upregulation of CD69, CD49a, and CD11a, and downregulation of CCR7, CD62L, SIPR1, and Klf2[40, 51, 52]. CD103, which is expressed by some CD8$^+$ Trm subsets, is rarely detected on lung CD4$^+$ Trm cells including Th2 Trm cells[41, 44, 52]. Instead, Th2 Trm cells express ST2[15, 42, 44, 45]. As expected, the Th2 Trm cell subset showed a signature of tissue residency, as evidenced by their diminished expression of *S1pr1*, *Ccr7*, and *Klf2* and enhanced expression of *Cd69* (Fig. 4e). To validate our transcriptomic data that Th2 Trm cells are increased in absence of HDAC1 (Fig. 4b), we performed flow cytometric analysis of lung cells from WT and HDAC1-cKO mice exposed to HDM or PBS. We confirmed that, loss of HDAC1 resulted in increased lung Th2 Trm cells (Fig. 4f-h). Importantly, given the increased proportion of HDAC1-cKO cells in the Th2 Trm cell subset (Fig. 4b, bottom) and in the lungs of HDAC1-cKO mice exposed to HDM (Fig. 4f-h), it is conceivable that HDAC1 plays a critical role in regulating the molecular processes involved in the formation of Th2 Trm cells. Collectively, these data underline the importance of HDAC1 in restraining the pathogenicity of lung pTh2 cell subsets as well as in the formation of Th2 Trm cells.

Lung pTh2 subsets exhibit shared and distinct transcriptional signatures

To better characterise the transcriptional signatures of lung pTh2 cell subsets, we compared each pTh2 cluster (peTh2 and Th2 Trm) with all other clusters. Our comparison revealed enrichment of transcriptional regulators such as *Bhlhe40*, *Gadd45b*, *Gata3*, *Pparg*, *Rbpj*, *Socs2*, *Hlf*, *Rgs1*, *Nfat5*, and *Zeb2* in both pTh2 cell subsets (Fig. 5a, b and Supplementary Table 4). Previous studies have demonstrated important roles for *Pparg*, *Bhlhe40*, and *Nfat5* in regulating type 2 cytokine production[16,

[17, 53, 54, 55, 56]. It will be crucial to further investigate the role of these transcriptional regulators in pTh2 cell differentiation particularly in Th2 Trm formation and maintenance.

Next, we compared the peTh2 cell subset with the Th2 Trm cell subset to define subset-specific gene signature. Interestingly, despite their overlapping transcriptional signatures, they differ in the expression of specific genes. The peTh2 cell subset was more enriched for effector molecules such as *Il4*, *Il5*, *Il10*, *Il13*, *Tnfsf11 (Rankl)*, *Areg*, and *Calca*, as well as several members of the tumor necrosis factor receptor superfamily (TNFRSF) *Tnfrsf4* (OX40), *Tnfrsf9* (4-1BB), and *Tnfrsf18* (GITR) (Fig. 5c and Supplementary Table 5). In contrast to the peTh2 cell subset, the Th2 Trm cell subset showed diminished expression of pathogenic effector molecules, and an enrichment of *Lpar6* and *Slc38a2*, which are known to modulate lysophosphatidic acid and amino acid metabolism[57, 58, 59], as well as *Zfp36l2* (Fig. 5c and Supplementary Table 5). The Th2 Trm cell subset also showed increased expression of transcriptional regulators of the activated protein-1 (AP-1) family *Fos*, *Fosb*, and *Jun* (Fig. 5c, d).

We further performed GSEA to define the pathways enriched in the pTh2 cell subsets compared with other $CD4^+$ T cells. Our analysis revealed an enrichment of similar pathways in both pTh2 cell subsets (Fig. 5e, f and Supplementary Table 6). Notably, the IL-2/STAT5 and TNF-α/NF-κB signalling pathways were among the most upregulated. Further assessment of the IL-2/STAT5 and TNF-α/NF-κB leading-edge genes (the core genes that contribute to the enrichment of these pathways) in the peTh2 cells (Fig. 5g, h and Supplementary Table 6), revealed enhanced expression of genes associated with TNF (*Tnfrsf4*, *Tnfrsf9*, *Tnfrsf18*, *Traf1*), mitogen-activated protein kinase (MAPK; *Map2k3*, Mapkapk2), AP-1 (*Fosl2*, *Batf*), and nuclear factor-κB (NF-κB; *Nfkb1*, *Rel*) signalling (Fig. 5h, i). These signalling components are known to regulate various cellular processes such as survival, stress response, proliferation, and differentiation[60, 61], but their role in pTh2 cell differentiation and effector function is unclear. Together, our analyses unveil the transcriptional profiles of lung peTh2 and Th2 Trm cells and identify mediators associated with their differentiation and effector function.

Co-stimulation of GITR and TSLPR drives *in vitro* differentiation of pTh2 cells

A major limitation to our understanding of how pTh2 cells are regulated is the lack of an appropriate system to generate and investigate them *in vitro*. We observed that lung peTh2 cells were highly enriched for *Tnfrsf4*, *Tnfrsf9*, and *Tnfrsf18*, members of the TNFRSF[62]. Specifically, the activation of TNFRSF18 also called glucocorticoid-induced TNFR family-related protein (GITR), has been shown to promote the features of allergic asthma and the differentiation of Th2 cells *in vitro*[63, 64, 65]. In addition, we found upregulation of the IL-2/STAT5 pathway in both pTh2 cell subsets. Previous studies have shown that the epithelial-derived cytokine, thymic stromal lymphopoietin (TSLP), promotes pathogenic features in *in vitro* differentiated Th2 cells via the activation of STAT5 (refs.[66, 67]). Therefore, our data and previous work suggest that co-stimulation of GITR and/or TSLP receptor (TSLPR) could induce the *in vitro* generation of pTh2 cells. To test our hypothesis, we differentiated naïve $CD4^+$ T cells under Th2-promoting conditions alone (Fig. 6a, left), or in the presence of TSLP alone, a GITR agonist (DTA-1) alone, or in combination (Fig. 6a, right). Our flow cytometric analyses revealed that both the GITR agonist and TSLP induced IL-4 and IL-13 expression in the Th2 cells, with the GITR agonist being more potent in inducing IL-13 expression (Fig. 6b, c). However, a combination of both stimuli resulted in higher expression of IL-4 and IL-13 (Fig. 6b, c). Remarkably, the level of IL-5 was more pronounced when both the GITR agonist and TSLP were combined (Fig. 6d, e). Importantly, the deletion of HDAC1 resulted in an augmented expression of the pathogenic Th2 cytokines compared with WT cells (Fig. 6b-e) despite comparable GATA3 protein levels (Fig. 6f, g). The *in vitro* generated pTh2 cells also showed enhanced expression of RANKL, GM-CSF, and IL-9 (Extended Data Fig. 5a-c). These results indicate that co-stimulation of GITR and TSLPR promotes *in vitro* differentiation of pTh2 cells.

We also assessed the impact of TNFRSF4 (OX40) and TNFRSF9 (4-1BB) co-stimulation on Th2 cell differentiation. Using anti-mouse OX40 and 4-1BB agonistic antibodies together with TSLP, we found

that OX40 co-stimulation had a minimal effect in inducing pathogenic features in the *in vitro* differentiated Th2 cells (Extended Data Fig. 5d, e). Unlike OX40, 4-1BB co-stimulation led to enhanced expression of pathogenic cytokines (Extended Data Fig. 5d, e). Although 4-1BB co-stimulation promoted the expression of pathogenic cytokines, it was less potent than GITR co-stimulation (Extended Data Fig. 5d, e). Collectively, these results reveal the crucial role of the TNFRSF members GITR and 4-1BB in driving Th2 cells towards a pathogenic state. Notably, we demonstrate that co-stimulation of GITR and TSLPR promotes the acquisition of strong pathogenic features in Th2 cells and represents a novel strategy to generate pTh2 *in vitro*. Our results further demonstrate that HDAC1 is essential to restrict the acquisition of pathogenic features, particularly IL-5, in cells differentiated under pTh2-promoting conditions.

Combined transcriptome and proteome profiling reveals a shared signature between *in vitro* generated pTh2 and lung peTh2 cells

Next, we performed bulk RNA-seq to better define the transcriptional profile of pTh2 cells generated *in vitro* and to compare them with lung pTh2 cell subsets (Fig. 7a). Differential gene expression analysis of *in vitro* WT pTh2 and WT Th2 cells revealed upregulation of key pathogenic signature genes including *Bhlhe40*, *Pparg*, *Gadd45b*, *Zeb2*, *Atf3*, *Areg*, *Csf2, Il4*, *Il5*, *Il9*, and *Il13* in pTh2 cells (Fig. 7b and Supplementary Table 7). A similar transcriptional signature was observed in HDAC1-cKO pTh2 cells compared with HDAC1-cKO Th2 cells (Fig. 7c and Supplementary Table 7). Absence of HDAC1 augmented the expression of pathogenic molecules (*Il5*, *Il13*, *Bhlhe40*) in Th2 and pTh2 cells compared with WT Th2 and pTh2 cells, respectively (Extended Data Fig. 6a, b).

To determine whether the *in vitro* pTh2 cells exhibit a similar transcriptional signature as lung pTh2 cells, we first compared the lung peTh2 gene set (Supplementary Table 2) with gene sets from *in vitro* pTh2 and Th2 cells (Supplementary Table 7). Our GSEA revealed that both WT and HDAC1-cKO *in vitro* pTh2 cells were highly enriched for lung peTh2 signature as compared with their corresponding Th2 cells (Fig. 7d, e and Supplementary Table 8). Next, we took the leading-edge genes (the core genes that contribute to the enrichment of peTh2 signature) in WT pTh2 cells (Fig. 7d) and examined their expression profile across the *in vitro* Th2 and pTh2 cells from WT and HDAC1-cKO. Our analysis revealed that these leading-edge genes are distinctively expressed by pTh2 cells as compared with Th2 cells (Extended Data Fig. 6c and Supplementary Table 9). Thus, these genes represent the core pathogenic Th2 signature genes since they are highly enriched in lung peTh2 cells and *in vitro* pTh2 cells. Notably, some of the core pathogenic Th2 signature genes including *Il5*, *Il13*, *Bhlhe40*, *Map2k3*, and *Mapkapk2* were also upregulated in HDAC1-cKO Th2 cells (Extended Data Fig. 6c), indicating that these cells have already acquired a pathogenic signature. Consistently, the HDAC1-cKO Th2 were also enriched for genes from the lung peTh2 gene set as compared with the WT Th2 cells (Fig. 7f and Supplementary Table 8), demonstrating that the absence of HDAC1 predisposes the *in vitro* Th2 cells to acquire a pathogenic program. These results further underline the crucial role of HDAC1 in restraining the differentiation of pTh2 cells. We further compared the *in vitro* pTh2 cells with lung Th2 Trm cells. Although the *in vitro* pTh2 cells shared some features with lung Th2 Trm cells, their similarity was less pronounced (Extended Data Fig. 6d-f and Supplementary Table 8) as compared with the lung peTh2 cells (Fig. 7d-f). This is expected as the Th2 Trm cells already acquired tissue residency features with diminished effector program (Fig. 4d, e). Overall, these results indicate that the pTh2 cells we have generated *in vitro* are highly comparable to lung peTh2 cells. Of note, the *in vitro* generated pTh2 cells do not express *Il1rl1* (ST2), indicating that our culture conditions are insufficient to induce ST2. Thus, additional signal (s), or longer time in culture might be required for ST2 expression as previously demonstrated[68]. Nonetheless, the *in vitro* pTh2 cells also showed an enrichment of similar pathways as the lung pTh2 cell subsets, notably, the IL-2/STAT5 and TNF-α/NF-κB pathways (Extended Data Fig. 6g, h and supplementary 10).

Our transcriptomic analyses revealed that lung and *in vitro* generated pTh2 cells are highly enriched in components of the AP-1, MAPK, and NF-κB pathways (Fig. 5h, i and Extended Data Fig. 6c). To validate these findings on protein level, we performed proteomic analysis by quantitative mass spectrometry using the *in vitro* generated pTh2 cells (Fig. 7g). Consistent with our transcriptomic findings, our proteomic analysis revealed enrichment of proteins associated with AP-1, MAPK, and NF-κB signalling in the *in vitro* pTh2 cells (Fig. 7h-j and supplementary 11). Overall, these findings reveal that lung peTh2 cells and pTh2 cells generated *in vitro* have a similar transcriptional signature and rely on related gene regulatory networks for their differentiation.

The p38 MAPK pathway regulates IL-5 and IL-13 expression in pTh2 cells

Given that both lung and *in vitro* pTh2 cells showed upregulation of AP-1 and MAPK components, we assessed the impact of these pathways on pTh2 cell differentiation using small molecule inhibitors targeting AP-1 (T-5224) and p38 MAPK (SB 203580). SB 203580 markedly suppressed IL-5 and IL-13 expression in WT pTh2 without affecting IL-4 and GATA3 levels (Fig. 8a-c), and similar results were obtained using HDAC1-cKO pTh2 cells (Fig. 8d-f). Furthermore, SB 203580 suppressed the expression of GM-CSF and IL-9 in WT pTh2 cells (Extended Data Fig. 7a, b). In contrast, the inhibition of AP-1 with T-5224 did not affect WT and HDAC1-cKO pTh2 cell differentiation (Fig. 8a-f and Extended Data Fig. 7a, b). Moreover, targeting ERK1/2 and JNK signalling using the inhibitors U0126-EtoH and SP600125, respectively, did not affect pTh2 cell differentiation (Extended Data Fig. 7c, d). These results demonstrate that the p38 MAPK pathway selectively regulates IL-5 and IL-13 expression in pTh2 cells to restrict their differentiation.

Discussion

Unlike classical Th2 cells, pTh2 cells secrete high amounts of type 2 cytokines. They have become an important drug target in allergic asthma. Thus, defining the factors orchestrating their differentiation and pathogenicity is of great clinical importance. Our data resolve the heterogeneity of murine pTh2 cells, their transcriptional signatures, and uncover previously overlooked similarities between these cells and other lung ST2$^+$ Th cells. Additionally, we establish a new protocol to generate pTh2 cells *in vitro*, allowing the investigation of pathways and regulators critical for their differentiation. Furthermore, we find that HDAC1 is essential to restrict HDM-induced allergic asthma and the differentiation of lung and *in vitro* generated pTh2 cells (Extended Data Fig. 8).

Our scRNA-seq analysis reveals two distinct subsets of lung pTh2 cells: pathogenic effector Th2 (peTh2) and pathogenic Th2 tissue-resident memory (Th2 Trm) cells. Both subsets are highly proinflammatory and express various inflammatory cytokines and mediators such as *Il4*, *Il5*, *Il13*, *Tnfsf11*, *Areg*, *Tgfb1*, *Calca*, and *Furin*, all of which are implicated in promoting allergic asthma and other allergic diseases[1, 69, 70, 71, 72, 73, 74]. In addition, we identify a unique Th subset that has features of both Treg and Th2 cells (Treg/Th2). Intriguingly, the pTh2 cell subsets show some similarities with the Treg/Th2 cell subset. Many marker genes previously attributed to lung pTh2 cells such as *Il1rl1* (ST2), *Areg*, and *Bhlhe40* are not unique to the pTh2 cell subsets. Of note, previous studies in mice relied mostly on ST2 to define pTh2 cells[15, 18, 42, 43, 44, 45], however, a detailed characterisation of lung ST2$^+$ Th subsets in response to HDM is lacking. Our scRNA-seq analysis suggests that using ST2 alone is insufficient to define pTh2 cells since it is also expressed by Treg/Th2 cells, which we collectively termed non-pTh2 ST2$^+$ Th cells due to their high expression of FoxP3. Notably, to exclude FoxP3-expressing ST2$^+$ Th cells and obtain "pure" ST2$^+$ pTh2 cells, FoxP3 reporter mice could be used as previously demonstrated[45]. However, due to the laborious nature of acquiring and maintaining reporter mice as well as possible background problems arising from crossing different types of mouse strains, using surface markers might represent a generally applicable and unbiased approach. These limitations underline the need to define markers to clearly distinguish the different ST2$^+$ Th subsets. Thus, we identify surface markers distinctively expressed by the ST2$^+$ Th subsets and establish a flow cytometry gating strategy for distinguishing each subset. We anticipate that by using our proposed surface marker

panel, murine lung pTh2 cell subsets can be distinguished from the non-pTh2 ST2$^+$ Th subsets and purified for detailed functional and phenotypic characterisation.

Our work further reveals the shared and distinct transcriptional signatures of peTh2 and Th2 Trm cells. Both subsets express high levels of transcriptional regulators such as *Gata3*, *Bhlhe40*, *Pparg*, *Gadd45b*, and *Nfat5*. However, peTh2 cells exhibit more effector phenotype with increased expression of type 2 effector molecules than Th2 Trm cells. The reduced expression of these effector molecules in Th2 Trm cells suggests a distinct differentiation stages between these two pTh2 cell subsets. For instance, Th2 Trm cells show a diminished expression of *Il13* mRNA despite expressing the protein, suggesting that they already down-regulated/modulated *Il13* on a transcriptional level and indicating that they are more differentiated than peTh2 cells. This is further substantiated by their acquisition of a tissue-residency program such as enhanced expression of *Cd69* and reduced expression levels of *S1pr1*, *Klf2*, and *Ccr7*. Additionally, in contrast to peTh2 cells, lung Th2 Trm cells are enriched in *Zfp36l2*, *Lpar6*, *Slc38a2*, and *Egr1*. *Zfp36l2* encodes zinc finger protein 36 like 2 (Zfp36l2), which is an RNA-binding protein (RBP). RBPs bind the adenine-uridine-rich elements (AREs) in the 3´untranslated regions of many mRNAs to regulate gene expression[75] and are suggested to exhibit an anti-inflammatory role by restricting the expression of various proinflammatory molecules[76]. Interestingly, it has been demonstrated that *Zfp36l2* is essential to repress interferon-γ translation from pre-formed cytokine encoding RNA in mouse and human memory T cells, serving as a regulatory mechanism to limit aberrant cytokine secretion[77]. It is unclear what mechanism causes the diminished mRNA expression of effector molecules such as *Il13* in the Th2 Trm cell subset, but we speculate that *Zfp36l2* might play a role in this regulation to limit the excessive production of pathogenic molecules by these cells. Furthermore, Th2 Trm cells are highly enriched for *Fos*, *Fosb*, and *Jun*; members of the activator protein-1 (AP-1) transcription factor (TF) family[78]. Increased expression and accessibility of these TFs in skin CD8$^+$ Trm cells have been reported recently. Notably, deletion of *Fos* and *Fosb* impaired skin CD8$^+$ Trm formation[79]. Thus, our analyses identify novel metabolic and transcriptional regulators that warrant further investigation, especially in Th2 Trm formation and maintenance.

Our understanding of the molecular mechanisms regulating pTh2 cells is hindered by the lack of an *in vitro* model to generate and study them in more detail. Our data uncover that co-stimulation of GITR together with TSLPR, induces pTh2 differentiation *in vitro*. We confirm that these *in vitro* generated pTh2 cells are highly similar to lung peTh2 cells and exhibit enhanced upregulation of pathogenic molecules and TFs. Therefore, our work unravels the importance of co-stimulatory factors like ligands of TNFRSF members together with TSLP to drive the differentiation of pTh2 cells. GITR ligand is indeed upregulated in the peripheral blood of asthmatic children and on lung dendritic cells of HDM-exposed mice, suggesting a critical role of the GITR-GITRL axis in allergic asthma[65]. Furthermore, using our new *in vitro* model, we show that targeting p38 MAPK suppresses IL-5 and IL-13 expression in pTh2 cells. Our finding that the p38 MAPK pathway is crucial for pTh2 differentiation independently of IL-33 adds to previous studies demonstrating a role for this pathway in regulating IL-5 and IL-13 expression in both human and murine T cells[15, 80, 81, 82]. Since p38 MAPK has diverse effects and controls many physiological processes[83, 84, 85], inhibiting it may be deleterious. However, identifying its downstream targets and defining their role in pTh2 cell differentiation might potentially lead to better therapeutic targets for treating allergic asthma and other allergic diseases. We anticipate that our new *in vitro* model for generating pTh2 cells will be leveraged to strengthen our understanding of the molecular processes driving pTh2-mediated allergic asthma.

It is well established that epigenetic regulators such as HDACs play important roles in T cell biology[30, 31, 38]. Our work highlights the importance of HDAC1 in HDM-induced allergic asthma and pTh2 cell differentiation. Deletion of HDAC1 in T cells promotes HDM-induced airway inflammation and the pathogenicity of lung pTh2 cell subsets. In particular, HDAC1 dampens IL-5 production. In addition, HDAC1 appears to restrain Th2 Trm cell formation, as evidenced by the increased proportion of Th2 Trm cells in absence of HDAC1. Several lines of evidence implicate Th2 Trm cells as important players

in mediating allergic asthma due to their propensity to rapidly secrete effector molecules upon re-encounter with an allergen[15, 41, 44, 45, 49, 50]. Thus, identifying the mechanisms underlying their generation and maintenance is of great importance for developing new therapies for allergic asthma[45]. Moreover, consistent with our *in vivo* findings, HDAC1 is also essential to limit the pathogenicity of *in vitro* generated pTh2 cells, particularly IL-5. These findings have broad implications, as natural HDAC inhibitors such as short-chain fatty acids (SCFAs), derived from bacterial fermentation of non-digestible dietary fibre[36, 86, 87, 88], are regarded as immunosuppressive[89, 90, 91]. Subsequently, SCFAs are suggested as potential therapeutic agents to ameliorate various diseases including allergic asthma[92, 93, 94, 95, 96, 97, 98], at odds with the findings that they could augment type 2 cytokine production[99, 100], as well as promote allergic asthma[100]. Therefore, it is crucial to further investigate the effects of natural HDAC inhibitors like SCFAs on pTh2 cell differentiation and whether they are suitable candidates for treating allergic asthma. Based on our findings, augmenting the activity of HDAC1 might represent a novel approach to limiting allergic asthma. Overall, we have established an important link between HDAC1, pTh2 differentiation and allergic asthma. The mechanisms by which loss of HDAC1 favours the upregulation of pathogenic Th2 effector molecules and Th2 Trm cell formation remain to be determined.

Collectively, we resolve the heterogeneity of murine lung pTh2 cell subsets and reveal their transcriptional and phenotypic profiles. We identify a new system to generate pTh2 cells *in vitro*, which will be useful to delineate the molecular mechanisms critical for their pathogenicity. Our work further illustrates that HDAC1 is a master regulator of pTh2 cells, suggesting that therapeutic approaches aimed at inhibiting HDACs in allergic asthma, like the use of SCFAs, should be revisited. An in-depth understanding of how pTh2 cells are regulated will be crucial for developing novel therapies for pTh2-mediated allergic diseases including allergic asthma, allergic rhinitis, atopic dermatitis, eosinophilic esophagitis, and food allergy.

Methods

Mice

We used Hdac1$^{flox/flox}$ (HDAC1$^{f/f}$)[38], CD4-Cre[101], and IL-13tdTomato[39] mice. All mice were bred and maintained at the animal facility of the Medical University of Vienna. Animal husbandry and experiments were reviewed and approved by the Institutional Review Board of the Medical University of Vienna and approved by the Austrian Ministry of Economy and Science (BMWFW-2020-0.547.902) and performed as per the guidelines of the Federation of European Laboratory Animal Science Associations.

House dust mite model of allergic asthma

Eight to twelve weeks old female WT and HDAC1-cKO mice were sensitised intratracheally with 10 µg HDM (Greer Laboratories; Item no. XPB91D3A25, Lot no. 325470) in 40 µl phosphate buffer saline (PBS) at days 0 and 5. On days 12 and 14, the mice were challenged intranasally with 25 µg HDM in 40 µl PBS and euthanised on day 16. Control mice received 40 µl PBS alone during the sensitisation and challenge periods. All intratracheal and intranasal injections were performed under anaesthesia by intraperitoneal injection with ketamine plus xylazine or light inhalation of isoflurane, respectively.

Bronchoalveolar lavage (BAL) collection

To analyse immune cell infiltration in the lungs, BAL was obtained by flushing the lungs of each mouse three successive times with 1 ml PBS using a tracheal cannula. BAL samples were centrifuged, and red blood cell lysis was performed using 1x RBC lysis buffer (BioLegend, 420301). Total cells were determined using a Coulter counter (Beckman Coulter). The remaining cells were stained to identify eosinophils and other BAL cells by flow cytometry.

Isolation of lung cells

To prepare single-cell suspension from the lungs, each lung was perfused with PBS via the right ventricle, and then harvested. The lungs were minced and digested in RPMI-1640 (Sigma-Aldrich, R8758) containing 5% FCS (Biowest, S181H), 150 U/ml collagenase type I (Gibco, 17100-017), and 50 U/ml DNase I (Sigma-Aldrich, DN25) for 1 hour at 37ºC (with intermittent shaking every 15 minutes). A single-cell suspension was obtained by meshing digested lung tissue through a 70 µm cell strainer followed by washing with 2% FCS in PBS (FACS buffer). Red blood cell lysis was performed followed by washing and filtering the samples using a 40 µm strainer. The resulting single-cell suspension was used for further analysis.

Flow cytometry

Antibodies were purchased from eBioscience: TCRβ (H57-597), ST2 (RMST2-2), FoxP3(FJK-16s), IL-13(eBio 13A); BioLegend: Ly6G (1A8), CD19 (6D5), CD11b (M1/70), MHC class II (AF6-120.1), Siglec F (S17007L), F4/80 (BM8), CD11c (N418), CD4 (RM4-5), CD44 (IM7), KLRG1 (2F1/KLRG1), CD27 (LG.3A10), GATA3 (16E10A23), CD69 (H1.2F3), PD1 (29F.1A12), IL-4 (11B11), IL-5 (TRFK5), IL-9 (RM9A4), RANKL (IK22/5), GM-CSF (MP1-22E9); and BD Biosciences: CD62L (MEL-14), CD25 (PC61), CD8α (53-6.7), GATA3 (L50-823), CD44 (IM7).
For extracellular staining of lung and BAL cells, the cells were preincubated with anti-CD16/32 (Clone: 2.4G2, BD Biosciences, 553142) for 2 min to block FC receptors and prevent non-specific binding, followed by surface staining with a fixable viability dye (eBioscience) and antibodies. Extracellular staining was performed at 4ºC for 30 min, then followed by a washing step with FACS buffer, centrifugation and analysis, or intracellular staining for cytokine or transcription factor analysis.
For analyses requiring intracellular cytokine staining, cells were fixed with 100 µl fixation buffer (BioLegend, 420801) for 15 min, then washed with FACS buffer and permeabilised with 1X permeabilization buffer (BioLegend, 421002) for 45 min, without washing, antibodies were added directly into the tubes. Cells were incubated for another 45 min, then washed and analysed. The FoxP3 staining buffer kit (eBioscience, 00-5523-00) was used for *ex vivo* staining of transcription factors and used following the manufacturer's instructions. Stained cells were measured using LSRFortessa (BD Biosciences) and analysed by FlowJo (v.10.8.1, Tree Star)

***Ex vivo* restimulation of lung cells**

To detect cytokines in lung T cells, 6 x 10^6 lung cells were plated in a 6-well plate (Sarstedt, 83.3920) and restimulated with 50 ng/ml Phorbol 12-myristate 13-acetate (PMA) and 750 ng/ml ionomycin (both from Sigma-Aldrich) in the presence of GolgiPlug and GolgiStop (both from BD Biosciences) for 4h at 37 ºC. All cells were cultured in complete RPMI-1640 (RPMI-1640 supplemented with 10% FCS (Biowest, S181H), penicillin (100 U/ml) plus streptomycin (100 µg/ml) (Sigma-Aldrich, P0781), 2 mM Glutamax (Thermo Fisher Scientific, 35050038), 55 µM β-Mercaptoethanol (Sigma-Aldrich, M6250)). Intracellular cytokine staining was performed as described above and samples measured by flow cytometry.

Single-cell analysis of lung $CD4^+$ T cells

Sample preparation. Single-cell suspensions from lungs of WT and HDAC1-cKO IL-13 tdTomato reporter mice sensitised and challenged with HDM or PBS were extracellularly stained with a fixable viability dye and the following anti-mouse antibodies: CD19, CD8α, TCRβ, CD4, CD62L, CD44, and CD25. Cells were incubated at 4ºC for 30 min, then washed and centrifuged. Followed by cell sorting using BD FACSAria Fusion to sort for different $CD4^+$ T cell populations. To obtain the populations of interest, we first excluded all CD19 (B cells) and CD8α ($CD8^+$ cytotoxic T cells) positive cells and retained the $TCR\beta^+CD4^+$ T cells. Within the $CD4^+$ T cells, we further excluded the $CD25^{high}$ cells to enrich for non-Treg effector cells. We then sorted the following $CD4^+$ T cell populations: (1) naïve ($CD62L^+CD44^-$IL-13tdTomato$^-$), (2) IL-13^- Th cells ($CD62L^-CD44^+$IL-13tdTomato$^-$), and (3) IL-13^+ Th cells ($CD62L^-CD44^+$IL-13tdTomato$^+$). Naïve and IL-13^- Th cells were sorted from WT and HDAC1-cKO mice exposed to either PBS or HDM, while IL-13^+ Th cells were sorted only from WT and HDAC1-cKO mice exposed to HDM. We obtained a total of ten samples based on the two genotypes (WT and HDAC1-cKO) and experimental conditions (HDM and PBS) (see Fig. 1a). We pooled lung cells from three mice per group to enable us to sort sufficient number of cells. After sorting the populations of interest, we centrifuged the samples and resuspended them in 100 µl FACS buffer then incubated each sample with a unique hashtag oligonucleotide (HTO) antibody[102], using 0.5 µl HTO antibody (BioLegend) per sample. The samples were incubated at 4ºC for 30 min, followed by two washing steps, first with FACS buffer followed by 1 ml PBS containing 0.04% bovine serum albumin (BSA, Sigma-Aldrich). The samples were then resuspended in 100 µl PBS containing 0.04% BSA, and cells were counted. 3,000 cells were taken from each sample and pooled. A total of 30,000 cells (from 10 samples) were submitted for each scRNA-seq experiment.

Library preparation and sequencing. Single-cell suspensions were counted and diluted according to manufacturer recommendations before loading onto a Chromium Controller (10x Genomics, Pleasanton, CA, USA). Single-cell RNA-seq libraries were generated using the Next GEM Single Cell 3' Reagent Kit (v3.1, 10x Genomics, Pleasanton, CA, USA) according to the manufacturer's instructions aiming for a maximum cell recovery of 10,000 cells. NGS library concentrations were quantified with the Qubit 2.0 Fluorometric Quantitation system (Life Technologies, Carlsbad, CA, USA) and the size distribution was assessed using the 2100 Bioanalyzer instrument (Agilent, Santa Clara, CA, USA) before sequencing on a NovaSeq 6000 instrument (Illumina, San Diego, CA, USA). Both sequencing and data processing using the Cell Ranger suite (6.1.2, 10X Genomics, Pleasanton, CA, USA) was performed by the Biomedical Sequencing Facility at the CeMM Research Center for Molecular Medicine of the Austrian Academy of Sciences.

Analysis of scRNA-seq data. Subsequent analyses including demultiplexing, quality control, processing, integration, and visualisation were performed in R (v.4.1.2) using the Seurat package (v.4.0.6)[103]. For each dataset, HTO counts were first normalised using centered log-ration (CLR) transformation, followed by demultiplexing of the cells based on their origin (HTO labelling) using HTODemux. After demultiplexing, we excluded the negative cells and doublets and retained only the single cells for downstream analyses. Next, quality control was performed to exclude low-quality cells by excluding cells with more than 10% mitochondrial genes, and less than 200 or greater than 7500 features (genes). We then performed normalisation, feature selection, and data scaling. Each dataset

was normalised using the NormalizeData function based on the default parameters (using the "logNormalize" method and a scale factor of 10000). Highly variable genes were identified using the FindVariableFeatures function (using the "vst" method and top 2000 variable genes) and transformed the data with the ScaleData function. Next, principal components analysis (PCA) was performed with RunPCA to determine the dimensionality of the data followed by clustering of the cells using the FindNeighbors (on the first 20 principal components) and FindClusters (at a resolution of 1) functions. We then performed an additional step of doublet exclusion using DoubletFinder (v.2.0.3)[104], assuming a 7.6% doublet formation rate as recommended by 10x Genomics. After removing the doublets, we retained the singlets and performed normalisation, feature selection, data scaling, dimensionality reduction, and clustering, as previously mentioned. After processing each dataset separately, we merged them and performed normalisation, feature selection, data scaling, dimensionality reduction, and clustering, as previously mentioned. We then integrated both datasets by canonical correlation analysis (CCA) using the FindIntegrationAnchors and IntegrateData functions[105], then scaled the integrated data, performed dimensionality reduction, followed by clustering of the cells using FindNeighbors (on the first 15 principal components) and FindClusters (at a resolution of 0.5). The FindAllMarkers and FindMarkers functions were used to identify differentially expressed genes (DEGs) by only including genes that are expressed in at least 25% of the cells and with a minimum log fold change of 0.25 (min.pct = 0.25, logfc.threshold = 0.25). Statistical significance was determined using the default Wilcoxon rank sum test with Bonferroni correction. In addition to Seurat's visualisation tools, ggplot2 (v.3.4.0)[106], EnhancedVolcano (v.1.12.0)[107], scCustomized[108], and DeepVenn [http://www.deepvenn.com/] were also used. Gene set enrichment analysis[109] was performed in R using the fgsea package (v.1.20.0)[110]. The genes were pre-ranked based on avg_log2FC. To determine enriched pathways, we used the mouse HALLMARK gene set collection in The Molecular Signatures Database (MSigDB) (v.7.5.1)[111].

Mouse T helper cell differentiation

Single-cell suspensions were prepared from spleen and lymph nodes, then naïve $CD4^+$ T cells ($CD4^+CD62L^+CD44^-$) were isolated using the Miltenyi Naïve $CD4^+$ T cell isolation kit (Miltenyi Biotec, 130-104-453), and followed by purity check by flow cytometry. Isolated naïve $CD4^+$ T cells (1 x 10^5/ml) were plated in a 48-well plate (Sarstedt, 83.3923) precoated overnight at 4 ºC with 1 µg/ml anti-CD3ε (clone: 145-2C11, 553057) and 3 µg/ml anti-CD28 (clone: 37.51, 553294) both from BD Biosciences, and cultured in complete RPMI with different polarisation conditions. The following conditions were used for Th2 cell differentiation: IL-4 (25 ng/ml, Peprotech, 214-14), IL-2 (10 U/ml, Peprotech, AF-200-02), anti-IFN-γ (10 µg/ml, clone XMG1.2, BioXCell, BE0055), and anti-TGF-β1 (5 µg/ml, clone 1D11.16.8, BioXCell, BE0057). Th17: IL-6 (20 ng/ml, BioLegend, 575702), TGF-β1 (1 ng/ml, BioLegend, 580702). To investigate the induction of a pathogenic program in Th2 cells, naïve $CD4^+$ T cells were cultured under Th2-promoting conditions together with TSLP (50 ng/ml, R&D, 555-TS-010) and agonistic antibodies for GITR (5 µg/ml, clone DTA-1, BioXCell, BE0063), OX40 (5 µg/ml, clone OX-86, BioXCell, BE0031), or 4-1BB (5 µg/ml, clone 3H3, BE0239) all from BioXCell. Unless otherwise stated, $CD4^+$ T cells were cultured for 5 days, and on day 3 of culture, cells were passaged (1:2) in complete RPMI-1640 containing only anti-IFN-γ (10 µg/ml) and anti-TGF-β (5 µg/ml) without any activating or polarising conditions. To assess the role of activated protein-1 (AP-1) and mitogen-activated protein kinases (MAPKs) pathways, naïve $CD4^+$ T cells were cultured for 5 days under Th2-promoting conditions as above, and under pathogenic Th2 (pTh2)-promoting conditions: IL-4 (25 ng/ml), IL-2 (10 U/ml), TSLP (50 ng/ml), DTA-1 (5 µg/ml), anti-IFN-γ (10 µg/ml), and anti-TGF-β1 (5 µg/ml), and pTh2- promoting condition together with inhibitors for AP-1 (10 µM, T-5224, HY-12270), p38 (10 µM, SB 203580, HY-10256), Erk1/2 (1 µM, U0126-EtOH, HY-12031), or JNK (1 µM, SP600125, HY-12041) all from MedChemExpress. On day 3, cells were split (1:2) as indicated above. The inhibitors were added at the beginning of the experiments. For cytokine measurement, cultured cells were restimulated on day 5 with 50 ng/ml Phorbol 12-myristate 13-acetate (PMA) and 750 ng/ml ionomycin (both from Sigma-Aldrich) in the presence of GolgiPlug and GolgiStop (both from BD) for 4h at 37 ºC. Cells were then harvested, stained, and analysed by flow cytometry.

RNA-seq analysis of *in vitro* generated cells

Sample and library preparation for RNA-seq. Naïve $CD4^+$ T cells were isolated as previously described. Cells (1 x 10^5/ml) were plated in a 48-well plate (Sarstedt, 83.3923) precoated overnight at 4 ºC with 1 µg/ml anti-CD3ε and 3 µg/ml anti-CD28. Then cultured in complete RPMI under Th2-promoting conditions: IL-4 (25 ng/ml), IL-2 (10 U/ml), anti-IFN-γ (10 µg/ml), and anti-TGF-β1 (5 µg/ml) or pathogenic Th2 (pTh2)-promoting conditions: IL-4 (25 ng/ml), IL-2 (10 U/ml), TSLP (50 ng/ml), DTA-1 (5 µg/ml), anti-IFN-γ (10 µg/ml), and anti-TGF-β1 (5 µg/ml) for 3 days. On day 3, cells were harvested, and total RNA was isolated using the RNaesy Mini kit (Qiagen) according to the manufacturer's instructions.
The amount of total RNA was quantified using the Qubit 2.0 Fluorometric Quantitation system (Thermo Fisher Scientific, Waltham, MA, USA) and the RNA integrity number (RIN) was determined using the 2100 Bioanalyzer instrument (Agilent, Santa Clara, CA, USA). RNA-seq libraries were prepared with the TruSeq Stranded mRNA LT sample preparation kit (Illumina, San Diego, CA, USA) using Sciclone and Zephyr liquid handling workstations (PerkinElmer, Waltham, MA, USA) for pre- and post-PCR steps, respectively. Library concentrations were quantified with the Qubit 2.0 Fluorometric Quantitation system (Life Technologies, Carlsbad, CA, USA) and the size distribution was assessed using the 2100 Bioanalyzer instrument (Agilent, Santa Clara, CA, USA). For sequencing, samples were diluted and pooled into NGS libraries in equimolar amounts.

Sequencing and raw data acquisition. Expression profiling libraries were sequenced on a HiSeq 4000 instrument (Illumina, San Diego, CA, USA) following a 50-base-pair, single-end recipe. Raw data acquisition (HiSeq Control Software, HCS, HD 3.4.0.38) and base calling (Real-Time Analysis Software, RTA, 2.7.7) were performed on-instrument, while the subsequent raw data processing off the instruments involved two custom programs based on Picard tools (2.19.2). In the first step, base calls were converted into lane-specific, multiplexed, unaligned BAM files suitable for long-term archival (IlluminaBasecallsToMultiplexSam, 2.19.2-CeMM). In a second step, archive BAM files were demultiplexed into sample-specific, unaligned BAM files (IlluminaSamDemux, 2.19.2-CeMM).

Analysis of RNA-seq data. NGS reads were mapped to the Genome Reference Consortium GRCm38 assembly via "Spliced Transcripts Alignment to a Reference" (STAR, 2.7.5a)[112] utilising the "basic" Ensembl transcript annotation from version e100 (April 2020) as reference transcriptome. Since the mm10 assembly flavour of the UCSC Genome Browser was preferred for downstream data processing with Bioconductor packages for entirely technical reasons, Ensembl transcript annotation had to be adjusted to UCSC Genome Browser sequence region names. STAR was run with options recommended by the ENCODE project[113]. NGS read alignments overlapping Ensembl transcript features were counted with the Bioconductor (3.11) GenomicAlignments (1.24.0) package via the summarizeOverlaps function in Union mode, ignoring secondary alignments and alignments not passing vendor quality filtering. Since the Illumina TruSeq stranded mRNA protocol leads to the sequencing of the first strand, all alignments needed inverting before strand-specific counting in feature (i.e., gene, transcript, and exon) orientation. Transcript-level counts were aggregated to gene-level counts and the Bioconductor DESeq2 (1.28.1) package[114] was used to test for differential expression based on a model using the negative binomial distribution. Biologically meaningful results were extracted from the model, log2-fold values were shrunk with the ashr (2.2.-47) package[115], while two-tailed p-values obtained from Wald testing were adjusted with the Bioconductor Independent Hypothesis Weighting (IHW, 1.16.0) package[116]. The resulting gene lists were annotated and filtered for significantly differentially up-and down-regulated genes based on adjusted p value < 0.1. Plots were generated using ggplot2 (v.3.4.0) and EnhancedVolcano (v.1.12.0), and pheatmap (v.1.0.12). GSEA was performed in R using the fgsea package (v.1.20.0). The genes were pre-ranked based on log2FC. Pathway analysis was performed using the MSigDB (v.7.5.1) mouse HALLMARK gene set collection.

Proteomics analysis of *in vitro* generated cells

Cell and mass spectrometry sample preparation. Th2 and pTh2 cells were cultured as in the RNA-seq analysis. On day 3, the cells were harvested, washed pelleted before lysis.

Cells were resuspended in lysis buffer (8 M urea (VWR, 0568-500G), 50 mM Tris-HCl pH8.0, 150 mM NaCl, 1 mM PMSF, 5 mM sodium butyrate (Sigma-Aldrich,303410), 10 ng/ml NAM (Sigma Aldrich, 72340), 10 ng/ml trichostatin A (TSA) (Sigma Aldrich, T8552-1MG), 1x cOmplete protease inhibitor cocktail (+EDTA) (Roche, 11697498001), 250 U/replicate benzonase (Merck, 1.01695.0001)), lysed using a Bioruptor sonication device (Diagenode) (settings: 30 sec sonication (power level H, 30 sec cooling, 5 cycles), centrifuged for 10 min at 15,000 x g, 4°C and precipitated with 4x volumes of cold (-20°C) 100% acetone. Protein samples were washed with 80% acetone (-20°C), air dried, dissolved in 8 M urea, 50 mM ABC (Sigma Aldrich, 09830-500G), reduced in 10 mM DTT (Roche, 10197777001) for 45 min (RT), carbamidomethylated with 20 mM IAA (Sigma Aldrich, I6125-5G) for 30 min at RT in the dark, and quenched with 5 mM DTT for 10 min. The urea concentration was reduced to 4 M using 50 mM ABC. Samples were pre-digested with Lys-C (FUJIFILM Wako Pure Chemical Corporation, 125-02543) for 90 min at 37°C (enzyme-to-substrate ratio of 1:100) and subsequently digested overnight at 37°C with trypsin (Trypsin Gold, Mass Spec Grade, Promega, V5280) at an enzyme-to-substrate ratio of 1:50. Digests were stopped by acidification with TFA (Thermo Scientific, 28903) (0.5% final concentration) and desalted on a 50 mg tC18 Sep-Pak cartridge (Waters, WAT054960). Peptide concentrations were determined and adjusted according to UV chromatogram peaks obtained with an UltiMate 3000 Dual LC nano-HPLC System (Dionex, Thermo Fisher Scientific), equipped with a monolithic C18 column (Thermo). Desalted samples were lyophilized overnight.

Isobaric labelling using TMTpro 16plex. 300 µg of trypsin-digested and desalted peptides were used for each sample for isobaric labelling. Lyophilized peptides were dissolved in 20 µl 100 mM triethylammonium bicarbonate (TEAB) (Supelco, 18597-100ML). 500 µg of each TMT 10plex reagent (Thermo Scientific, 90110) were dissolved in 30 µl of acetonitrile (ACN) (VWR, 83639.320) and added to the peptide/TEAB mixes. Samples were labelled for 60 min at RT and small aliquots were checked for labelling efficiency. Reactions were quenched using hydroxylamine (Sigma Aldrich, 438227-50ML) (0.4% final concentration), pooled, desalted using Sep-Pak tC-18 (200 mg) cartridges (Waters, WAT054925), dried in a SpeedVac vacuum centrifuge (Eppendorf), and subsequently lyophilized overnight. Neutral pH fractionation was performed using a 60 min gradient of 4.5 to 45% ACN (VWR, 83639.320) in 10 mM ammonium formate (1ml formic acid (26N) (Merck, 1.11670.1000), 3ml ammonia (13N) (1.05432.1000) in 300ml H_2O, pH = 7 - 8, dilute 1:10) on an UltiMate 3000 Dual LC nano-HPLC System (Dionex, Thermo Fisher Scientific) equipped with an XBridge Peptide BEH C18 (130 Å, 3.5 µm, 4.6 mm x 250 mm) column (Waters) (flow rate of 1.0 ml/min). Fractions were collected and subsequently pooled in a non-contiguous manner into 8 pools and lyophilized overnight.

Mass spectrometry measurements. DDA-SPS-MS3 method with online real-time database search (RTS) was performed on an UltiMate 3000 Dual LC nano-HPLC System (Dionex, Thermo Fisher Scientific), containing both a trapping column for peptide concentration (PepMap C18, 5x 0.3 mm, 5 µm particle size) and an analytical column (PepMap C18, 500 x 0.075 µm, 2 µm particle size, Thermo Fisher Scientific), coupled to an Orbitrap Eclipse mass spectrometer (Thermo Fisher) via a FAIMS Pro Duo ion source (Thermo Fisher). The instrument was operated in data-dependent acquisition (DDA) mode with dynamic exclusion enabled. For peptide separation on the HPLC, the concentration of organic solvent (acetonitrile, VWR, 83639.320) was increased from 1.6% to 32% in 0.1% formic acid at a flow rate of 230 ml/min, using a 2-hour gradient time for proteome analysis. Peptides were ionised with a spray voltage of 2,4 kV. The instrument method included Orbitrap MS1 scans (resolution of 120,000; mass range 375−1,500 m/z; automatic gain control (AGC) target 4e5, max injection time of 50 ms, FAIMS CV -40V, -55V and -70V, dynamic exclusion 45 sec), and MS2 scans (CID collision energy of 30%; AGC target 1e4; rapid scan mode; max injection time of 50 ms, isolation window 1.2 m/z). RTS was enabled with full trypsin specificity, max. 2 missed cleavages, max. search time of 40 ms, max. 2 variable modifications, max. 10 peptides per protein, and considering the following modifications: Carbamidomethyl on cysteine and TMTpro16plex on Lys and peptide N-terminus as static, oxidation on Met and deamidation on Asn and Gln as variable modifications. The scoring thresholds were applied (1.4 for Xcorr, 0.1 for dCn, 10 ppm precursor tolerance) and the *Mus musculus* (mouse) Uniprot database (release 2020.01) was used for the search. Quantitative SPS-MS3 scans were performed in the Orbitrap with the following settings: HCD normalised collision energy 50%, resolution

50,000; AGC target 1.5e5; isolation window 1.2 m/Z, MS2 isolation window 3 m/z, 10 notches, max injection time of 150 ms. The total cycle time for each CV was set to 1.2 sec.

Mass spectrometry data analysis. MS raw files were split according to CVs (-40V, -55V, -70V) using FreeStyle 1.7 software (Thermo Scientific). Raw MS data were analysed using MaxQuant[117] software version 1.6.17.0, using default parameters with the following modifications. MS2 spectra were searched against *Mus musculus* (mouse) Uniprot database (release 2021.03; with isoforms) and a database of common laboratory contaminants. Enzyme specificity was set to "Trypsin/P", the minimal peptide length was set to 7 and the maximum number of missed cleavages was set to 2. Carbamidomethylation of cysteine was searched as a fixed modification. "Acetyl (Protein N-term)", "Oxidation (M)" were set as variable modifications. A maximum of 5 variable modifications per peptide was allowed. The identification and quantification information of proteins was obtained from the MaxQuant "ProteinGroups" tables. Data were analysed in R (4.1.0) using custom scripts. The analysis procedure covered: correction for isotopic impurities of labels, within-plex median normalisation, and statistical analysis between-group comparisons using LIMMA (3.50)[118]. Plots were generated using ggplot2 (v.3.4.0) and EnhancedVolcano (v.1.12.0), and pheatmap (v.1.0.12)[119].

Statistical analysis

Statistical analysis of non-omics data was performed in GraphPad Prism (v.9.3.1). Statistical significance between two groups was determined by a two-tailed unpaired Mann-Whitney *U* test. One-way or two-way ANOVA with Tukey's multiple comparisons test was used to compare more than two groups.

Data availability

Raw single-cell sequencing data were submitted to ArrayExpress (#E-MTAB-13089) and RNA-seq data to Gene Expression Omnibus. The mass spectrometry proteomics data have been deposited to the ProteomeXchange Consortium via the PRIDE[120] partner repository with the dataset identifier PXD042975. The authors declare that the data supporting the findings of this research are available in the article, the Supplementary Material, or on request from the corresponding author. All information will be available to editors and reviewers during reviewing/revision period and to the public after acceptance of the manuscript.

Code availability

Custom R-scripts used in the proteomics analysis have been deposited to the ProteomeXchange Consortium via the PRIDE[120] partner repository with the dataset identifier PXD042975. No custom code was used for the scRNA-seq analyses. Scripts will be shared upon request.

References:

1. Lambrecht, B.N. & Hammad, H. The immunology of asthma. *Nat Immunol* **16**, 45-56 (2015).
2. Komlosi, Z.I. *et al.* Cellular and molecular mechanisms of allergic asthma. *Mol Aspects Med* **85**, 100995 (2022).
3. Porsbjerg, C., Melen, E., Lehtimaki, L. & Shaw, D. Asthma. *Lancet* **401**, 858-873 (2023).
4. Leon, B. & Ballesteros-Tato, A. Modulating Th2 Cell Immunity for the Treatment of Asthma. *Front Immunol* **12**, 637948 (2021).
5. Willart, M.A. & Lambrecht, B.N. The danger within: endogenous danger signals, atopy and asthma. *Clin Exp Allergy* **39**, 12-19 (2009).
6. Calven, J., Ax, E. & Radinger, M. The Airway Epithelium-A Central Player in Asthma Pathogenesis. *Int J Mol Sci* **21** (2020).
7. Islam, S.A. & Luster, A.D. T cell homing to epithelial barriers in allergic disease. *Nat Med* **18**, 705-715 (2012).
8. Walker, J.A. & McKenzie, A.N.J. T(H)2 cell development and function. *Nat Rev Immunol* **18**, 121-133 (2018).
9. Mitson-Salazar, A. *et al.* Hematopoietic prostaglandin D synthase defines a proeosinophilic pathogenic effector human T(H)2 cell subpopulation with enhanced function. *J Allergy Clin Immunol* **137**, 907-918 e909 (2016).
10. Lam, E.P. *et al.* IL-25/IL-33-responsive TH2 cells characterize nasal polyps with a default TH17 signature in nasal mucosa. *J Allergy Clin Immunol* **137**, 1514-1524 (2016).
11. Seumois, G. *et al.* Transcriptional Profiling of Th2 Cells Identifies Pathogenic Features Associated with Asthma. *J Immunol* **197**, 655-664 (2016).
12. Wambre, E. *et al.* A phenotypically and functionally distinct human T(H)2 cell subpopulation is associated with allergic disorders. *Sci Transl Med* **9** (2017).
13. Vieira Braga, F.A. *et al.* A cellular census of human lungs identifies novel cell states in health and in asthma. *Nat Med* **25**, 1153-1163 (2019).
14. Islam, S.A. *et al.* Mouse CCL8, a CCR8 agonist, promotes atopic dermatitis by recruiting IL-5+ T(H)2 cells. *Nat Immunol* **12**, 167-177 (2011).
15. Endo, Y. *et al.* The interleukin-33-p38 kinase axis confers memory T helper 2 cell pathogenicity in the airway. *Immunity* **42**, 294-308 (2015).
16. Chen, T. *et al.* PPAR-gamma promotes type 2 immune responses in allergy and nematode infection. *Sci Immunol* **2** (2017).
17. Nobs, S.P. *et al.* PPARgamma in dendritic cells and T cells drives pathogenic type-2 effector responses in lung inflammation. *J Exp Med* **214**, 3015-3035 (2017).
18. Tibbitt, C.A. *et al.* Single-Cell RNA Sequencing of the T Helper Cell Response to House Dust Mites Defines a Distinct Gene Expression Signature in Airway Th2 Cells. *Immunity* **51**, 169-184 e165 (2019).
19. Ihara, F. *et al.* Identification of specifically reduced Th2 cell subsets in allergic rhinitis patients after sublingual immunotherapy. *Allergy* **73**, 1823-1832 (2018).
20. Morgan, D.M. *et al.* Clonally expanded, GPR15-expressing pathogenic effector T(H)2 cells are associated with eosinophilic esophagitis. *Sci Immunol* **6** (2021).
21. Bangert, C. *et al.* Persistence of mature dendritic cells, T(H)2A, and Tc2 cells characterize clinically resolved atopic dermatitis under IL-4Ralpha blockade. *Sci Immunol* **6** (2021).
22. Monian, B. *et al.* Peanut oral immunotherapy differentially suppresses clonally distinct subsets of T helper cells. *J Clin Invest* **132** (2022).
23. Nakayama, T. *et al.* Th2 Cells in Health and Disease. *Annu Rev Immunol* **35**, 53-84 (2017).
24. Mitson-Salazar, A. & Prussin, C. Pathogenic Effector Th2 Cells in Allergic Eosinophilic Inflammatory Disease. *Front Med (Lausanne)* **4**, 165 (2017).
25. Bertschi, N.L., Bazzini, C. & Schlapbach, C. The Concept of Pathogenic TH2 Cells: Collegium Internationale Allergologicum Update 2021. *Int Arch Allergy Immunol* **182**, 365-380 (2021).

26. Tripathi, S.K. & Lahesmaa, R. Transcriptional and epigenetic regulation of T-helper lineage specification. *Immunol Rev* **261**, 62-83 (2014).
27. Tumes, D.J. *et al.* Epigenetic regulation of T-helper cell differentiation, memory, and plasticity in allergic asthma. *Immunol Rev* **278**, 8-19 (2017).
28. Shakespear, M.R., Halili, M.A., Irvine, K.M., Fairlie, D.P. & Sweet, M.J. Histone deacetylases as regulators of inflammation and immunity. *Trends Immunol* **32**, 335-343 (2011).
29. Ellmeier, W. & Seiser, C. Histone deacetylase function in CD4(+) T cells. *Nat Rev Immunol* **18**, 617-634 (2018).
30. Moreira, J.M., Scheipers, P. & Sorensen, P. The histone deacetylase inhibitor Trichostatin A modulates CD4+ T cell responses. *BMC Cancer* **3**, 30 (2003).
31. Boucheron, N. *et al.* CD4(+) T cell lineage integrity is controlled by the histone deacetylases HDAC1 and HDAC2. *Nat Immunol* **15**, 439-448 (2014).
32. Stengel, K.R. *et al.* Histone Deacetylase 3 Is Required for Efficient T Cell Development. *Mol Cell Biol* **35**, 3854-3865 (2015).
33. Choi, J.H. *et al.* Trichostatin A attenuates airway inflammation in mouse asthma model. *Clin Exp Allergy* **35**, 89-96 (2005).
34. Bhavsar, P., Ahmad, T. & Adcock, I.M. The role of histone deacetylases in asthma and allergic diseases. *J Allergy Clin Immunol* **121**, 580-584 (2008).
35. Toki, S. *et al.* The histone deacetylase inhibitor trichostatin A suppresses murine innate allergic inflammation by blocking group 2 innate lymphoid cell (ILC2) activation. *Thorax* **71**, 633-645 (2016).
36. Bassett, S.A. & Barnett, M.P. The role of dietary histone deacetylases (HDACs) inhibitors in health and disease. *Nutrients* **6**, 4273-4301 (2014).
37. Yip, W. *et al.* Butyrate Shapes Immune Cell Fate and Function in Allergic Asthma. *Front Immunol* **12**, 628453 (2021).
38. Grausenburger, R. *et al.* Conditional deletion of histone deacetylase 1 in T cells leads to enhanced airway inflammation and increased Th2 cytokine production. *J Immunol* **185**, 3489-3497 (2010).
39. Barlow, J.L. *et al.* Innate IL-13-producing nuocytes arise during allergic lung inflammation and contribute to airways hyperreactivity. *J Allergy Clin Immunol* **129**, 191-198 e191-194 (2012).
40. Kumar, B.V. *et al.* Human Tissue-Resident Memory T Cells Are Defined by Core Transcriptional and Functional Signatures in Lymphoid and Mucosal Sites. *Cell Rep* **20**, 2921-2934 (2017).
41. Hondowicz, B.D. *et al.* Interleukin-2-Dependent Allergen-Specific Tissue-Resident Memory Cells Drive Asthma. *Immunity* **44**, 155-166 (2016).
42. Kobayashi, T., Iijima, K., Matsumoto, K., Lama, J.K. & Kita, H. Lung-resident CD69(+)ST2(+) T(H)2 cells mediate long-term type 2 memory to inhaled antigen in mice. *J Allergy Clin Immunol* (2023).
43. Morimoto, Y. *et al.* Amphiregulin-Producing Pathogenic Memory T Helper 2 Cells Instruct Eosinophils to Secrete Osteopontin and Facilitate Airway Fibrosis. *Immunity* **49**, 134-150 e136 (2018).
44. Bosnjak, B., Kazemi, S., Altenburger, L.M., Mokrovic, G. & Epstein, M.M. Th2-T(RMs) Maintain Life-Long Allergic Memory in Experimental Asthma in Mice. *Front Immunol* **10**, 840 (2019).
45. Rahimi, R.A., Nepal, K., Cetinbas, M., Sadreyev, R.I. & Luster, A.D. Distinct functions of tissue-resident and circulating memory Th2 cells in allergic airway disease. *J Exp Med* **217** (2020).
46. Wambre, E. *et al.* Differentiation stage determines pathologic and protective allergen-specific CD4+ T-cell outcomes during specific immunotherapy. *J Allergy Clin Immunol* **129**, 544-551, 551 e541-547 (2012).
47. Calise, J. *et al.* Optimal human pathogenic T(H)2 cell effector function requires local epithelial cytokine signaling. *J Allergy Clin Immunol* **148**, 867-875 e864 (2021).
48. Lozano-Ojalvo, D. *et al.* Allergen recognition by specific effector Th2 cells enables IL-2-dependent activation of regulatory T-cell responses in humans. *Allergy* **78**, 697-713 (2023).

49. Mojtabavi, N., Dekan, G., Stingl, G. & Epstein, M.M. Long-lived Th2 memory in experimental allergic asthma. *J Immunol* **169**, 4788-4796 (2002).
50. Turner, D.L. *et al.* Biased Generation and In Situ Activation of Lung Tissue-Resident Memory CD4 T Cells in the Pathogenesis of Allergic Asthma. *J Immunol* **200**, 1561-1569 (2018).
51. Zheng, M.Z.M. & Wakim, L.M. Tissue resident memory T cells in the respiratory tract. *Mucosal Immunol* **15**, 379-388 (2022).
52. Kunzli, M. & Masopust, D. CD4(+) T cell memory. *Nat Immunol* **24**, 903-914 (2023).
53. Micosse, C. *et al.* Human "T(H)9" cells are a subpopulation of PPAR-gamma(+) T(H)2 cells. *Sci Immunol* **4** (2019).
54. Henriksson, J. *et al.* Genome-wide CRISPR Screens in T Helper Cells Reveal Pervasive Crosstalk between Activation and Differentiation. *Cell* **176**, 882-896 e818 (2019).
55. Matthias, J. *et al.* Sodium chloride is an ionic checkpoint for human T(H)2 cells and shapes the atopic skin microenvironment. *Sci Transl Med* **11** (2019).
56. Jarjour, N.N. *et al.* BHLHE40 Promotes T(H)2 Cell-Mediated Antihelminth Immunity and Reveals Cooperative CSF2RB Family Cytokines. *J Immunol* **204**, 923-932 (2020).
57. Geraldo, L.H.M. *et al.* Role of lysophosphatidic acid and its receptors in health and disease: novel therapeutic strategies. *Signal Transduct Target Ther* **6**, 45 (2021).
58. Meyer zu Heringdorf, D. & Jakobs, K.H. Lysophospholipid receptors: signalling, pharmacology and regulation by lysophospholipid metabolism. *Biochim Biophys Acta* **1768**, 923-940 (2007).
59. Wang, W. & Zou, W. Amino Acids and Their Transporters in T Cell Immunity and Cancer Therapy. *Mol Cell* **80**, 384-395 (2020).
60. Zhang, W. & Liu, H.T. MAPK signal pathways in the regulation of cell proliferation in mammalian cells. *Cell Res* **12**, 9-18 (2002).
61. Liu, T., Zhang, L., Joo, D. & Sun, S.C. NF-kappaB signaling in inflammation. *Signal Transduct Target Ther* **2**, 17023- (2017).
62. Ward-Kavanagh, L.K., Lin, W.W., Sedy, J.R. & Ware, C.F. The TNF Receptor Superfamily in Co-stimulating and Co-inhibitory Responses. *Immunity* **44**, 1005-1019 (2016).
63. Patel, M. *et al.* Glucocorticoid-induced TNFR family-related protein (GITR) activation exacerbates murine asthma and collagen-induced arthritis. *Eur J Immunol* **35**, 3581-3590 (2005).
64. Motta, A.C. *et al.* GITR signaling potentiates airway hyperresponsiveness by enhancing Th2 cell activity in a mouse model of asthma. *Respir Res* **10**, 93 (2009).
65. Wang, Y. *et al.* GITRL on dendritic cells aggravates house dust mite-induced airway inflammation and airway hyperresponsiveness by modulating CD4(+) T cell differentiation. *Respir Res* **22**, 46 (2021).
66. Kitajima, M., Lee, H.C., Nakayama, T. & Ziegler, S.F. TSLP enhances the function of helper type 2 cells. *Eur J Immunol* **41**, 1862-1871 (2011).
67. Rochman, Y. *et al.* TSLP signaling in CD4(+) T cells programs a pathogenic T helper 2 cell state. *Sci Signal* **11** (2018).
68. Meisel, C. *et al.* Regulation and function of T1/ST2 expression on CD4+ T cells: induction of type 2 cytokine production by T1/ST2 cross-linking. *J Immunol* **166**, 3143-3150 (2001).
69. Locksley, R.M. Asthma and allergic inflammation. *Cell* **140**, 777-783 (2010).
70. Lambrecht, B.N., Hammad, H. & Fahy, J.V. The Cytokines of Asthma. *Immunity* **50**, 975-991 (2019).
71. Gregorczyk, I., Jasiecka-Mikolajczyk, A. & Maslanka, T. Blockade of NF-kappaB Translocation and of RANKL/RANK Interaction Decreases the Frequency of Th2 and Th17 Cells Capable of IL-4 and IL-17 Production, Respectively, in a Mouse Model of Allergic Asthma. *Molecules* **26** (2021).
72. Busse, W.W. *et al.* Understanding the key issues in the treatment of uncontrolled persistent asthma with type 2 inflammation. *Eur Respir J* **58** (2021).

73. Okano, M. *et al.* Interleukin-33-activated neuropeptide CGRP-producing memory Th2 cells cooperate with somatosensory neurons to induce conjunctival itch. *Immunity* **55**, 2352-2368 e2357 (2022).
74. Srisomboon, Y. *et al.* Allergen-induced DNA release by the airway epithelium amplifies type 2 immunity. *J Allergy Clin Immunol* **151**, 494-508 e496 (2023).
75. Turner, M. & Diaz-Munoz, M.D. RNA-binding proteins control gene expression and cell fate in the immune system. *Nat Immunol* **19**, 120-129 (2018).
76. Liu, J. & Cao, X. RBP-RNA interactions in the control of autoimmunity and autoinflammation. *Cell Res* **33**, 97-115 (2023).
77. Salerno, F. *et al.* Translational repression of pre-formed cytokine-encoding mRNA prevents chronic activation of memory T cells. *Nat Immunol* **19**, 828-837 (2018).
78. Garces de Los Fayos Alonso, I. *et al.* The Role of Activator Protein-1 (AP-1) Family Members in CD30-Positive Lymphomas. *Cancers (Basel)* **10** (2018).
79. Buquicchio, F.A. *et al.* A unique epigenomic landscape defines CD8(+) tissue-resident memory T cells. *bioRxiv*, 2022.2005.2004.490680 (2022).
80. Mori, A. *et al.* p38 mitogen-activated protein kinase regulates human T cell IL-5 synthesis. *J Immunol* **163**, 4763-4771 (1999).
81. Harlin, H., Podack, E., Boothby, M. & Alegre, M.L. TCR-independent CD30 signaling selectively induces IL-13 production via a TNF receptor-associated factor/p38 mitogen-activated protein kinase-dependent mechanism. *J Immunol* **169**, 2451-2459 (2002).
82. Guo, L. *et al.* IL-1 family members and STAT activators induce cytokine production by Th2, Th17, and Th1 cells. *Proc Natl Acad Sci U S A* **106**, 13463-13468 (2009).
83. Dodeller, F. & Schulze-Koops, H. The p38 mitogen-activated protein kinase signaling cascade in CD4 T cells. *Arthritis Res Ther* **8**, 205 (2006).
84. Cuenda, A. & Rousseau, S. p38 MAP-kinases pathway regulation, function and role in human diseases. *Biochim Biophys Acta* **1773**, 1358-1375 (2007).
85. Canovas, B. & Nebreda, A.R. Diversity and versatility of p38 kinase signalling in health and disease. *Nat Rev Mol Cell Biol* **22**, 346-366 (2021).
86. Wong, J.M., de Souza, R., Kendall, C.W., Emam, A. & Jenkins, D.J. Colonic health: fermentation and short chain fatty acids. *J Clin Gastroenterol* **40**, 235-243 (2006).
87. Belkaid, Y. & Hand, T.W. Role of the microbiota in immunity and inflammation. *Cell* **157**, 121-141 (2014).
88. Thorburn, A.N., Macia, L. & Mackay, C.R. Diet, metabolites, and "western-lifestyle" inflammatory diseases. *Immunity* **40**, 833-842 (2014).
89. Maslowski, K.M. *et al.* Regulation of inflammatory responses by gut microbiota and chemoattractant receptor GPR43. *Nature* **461**, 1282-1286 (2009).
90. Smith, P.M. *et al.* The microbial metabolites, short-chain fatty acids, regulate colonic Treg cell homeostasis. *Science* **341**, 569-573 (2013).
91. Arpaia, N. *et al.* Metabolites produced by commensal bacteria promote peripheral regulatory T-cell generation. *Nature* **504**, 451-455 (2013).
92. Trompette, A. *et al.* Gut microbiota metabolism of dietary fiber influences allergic airway disease and hematopoiesis. *Nat Med* **20**, 159-166 (2014).
93. Thorburn, A.N. *et al.* Evidence that asthma is a developmental origin disease influenced by maternal diet and bacterial metabolites. *Nat Commun* **6**, 7320 (2015).
94. Marino, E. *et al.* Gut microbial metabolites limit the frequency of autoimmune T cells and protect against type 1 diabetes. *Nat Immunol* **18**, 552-562 (2017).
95. Li, M., van Esch, B., Henricks, P.A.J., Folkerts, G. & Garssen, J. The Anti-inflammatory Effects of Short Chain Fatty Acids on Lipopolysaccharide- or Tumor Necrosis Factor alpha-Stimulated Endothelial Cells via Activation of GPR41/43 and Inhibition of HDACs. *Front Pharmacol* **9**, 533 (2018).

96. Cait, A. *et al.* Microbiome-driven allergic lung inflammation is ameliorated by short-chain fatty acids. *Mucosal Immunol* **11**, 785-795 (2018).
97. Vieira, R.S. *et al.* Butyrate Attenuates Lung Inflammation by Negatively Modulating Th9 Cells. *Front Immunol* **10**, 67 (2019).
98. Theiler, A. *et al.* Butyrate ameliorates allergic airway inflammation by limiting eosinophil trafficking and survival. *J Allergy Clin Immunol* **144**, 764-776 (2019).
99. Han, S. *et al.* HDAC inhibitors TSA and sodium butyrate enhanced the human IL-5 expression by altering histone acetylation status at its promoter region. *Immunol Lett* **108**, 143-150 (2007).
100. Wen, T. *et al.* Single-cell RNA sequencing identifies inflammatory tissue T cells in eosinophilic esophagitis. *J Clin Invest* **129**, 2014-2028 (2019).
101. Lee, P.P. *et al.* A critical role for Dnmt1 and DNA methylation in T cell development, function, and survival. *Immunity* **15**, 763-774 (2001).
102. Stoeckius, M. *et al.* Cell Hashing with barcoded antibodies enables multiplexing and doublet detection for single cell genomics. *Genome Biol* **19**, 224 (2018).
103. Hao, Y. *et al.* Integrated analysis of multimodal single-cell data. *Cell* **184**, 3573-3587 e3529 (2021).
104. McGinnis, C.S., Murrow, L.M. & Gartner, Z.J. DoubletFinder: Doublet Detection in Single-Cell RNA Sequencing Data Using Artificial Nearest Neighbors. *Cell Syst* **8**, 329-337 e324 (2019).
105. Stuart, T. *et al.* Comprehensive Integration of Single-Cell Data. *Cell* **177**, 1888-1902 e1821 (2019).
106. Wickham, H. ggplot2:Elegant Graphics for Data Analysis. (Springer, 2016).
107. Kevin Blighe, S.R., Myles Lewis. EnhancedVolcano: Publication-ready volcano plots with enhanced colouring and labeling. (2021).
108. Marsh, S. scCustomize: Custom Visualizations & Functions for Streamlined Analyses of Single Cell. (2023).
109. Subramanian, A. *et al.* Gene set enrichment analysis: a knowledge-based approach for interpreting genome-wide expression profiles. *Proc Natl Acad Sci U S A* **102**, 15545-15550 (2005).
110. Korotkevich, G. *et al.* Fast gene set enrichment analysis. *bioRxiv*, 060012 (2021).
111. Liberzon, A. *et al.* The Molecular Signatures Database (MSigDB) hallmark gene set collection. *Cell Syst* **1**, 417-425 (2015).
112. Dobin, A. *et al.* STAR: ultrafast universal RNA-seq aligner. *Bioinformatics* **29**, 15-21 (2013).
113. Consortium, E.P. An integrated encyclopedia of DNA elements in the human genome. *Nature* **489**, 57-74 (2012).
114. Love, M.I., Huber, W. & Anders, S. Moderated estimation of fold change and dispersion for RNA-seq data with DESeq2. *Genome Biol* **15**, 550 (2014).
115. Stephens, M. False discovery rates: a new deal. *Biostatistics* **18**, 275-294 (2017).
116. Ignatiadis, N., Klaus, B., Zaugg, J.B. & Huber, W. Data-driven hypothesis weighting increases detection power in genome-scale multiple testing. *Nat Methods* **13**, 577-580 (2016).
117. Cox, J. & Mann, M. MaxQuant enables high peptide identification rates, individualized p.p.b.-range mass accuracies and proteome-wide protein quantification. *Nat Biotechnol* **26**, 1367-1372 (2008).
118. Ritchie, M.E. *et al.* limma powers differential expression analyses for RNA-sequencing and microarray studies. *Nucleic Acids Res* **43**, e47 (2015).
119. Kolde, R. pheatmap: Pretty Heatmaps. (2019).
120. Perez-Riverol, Y. *et al.* The PRIDE database resources in 2022: a hub for mass spectrometry-based proteomics evidences. *Nucleic Acids Res* **50**, D543-D552 (2022).

Acknowledgements

We thank the Biomedical Sequencing Facility at CeMM for assistance with next-generation sequencing and Michael Schuster for initial data processing and analysis of RNA-seq data. Mice were kept at the Core facility laboratory animal breeding and husbandry of the Medical University of Vienna. We also thank Dieter Printz of the FACS Core Unit at St. Anna CCRI for cell sorting. We are thankful to Shinya Sakaguchi for critical reading of the manuscript. We are grateful to Sahar Kazemi and Michelle Epstein for useful discussions on animal experiments and conceptual guidance in the allergy research field. This study has been funded by Austrian Science Foundation (FWF) through projects P30885 and F7004.

Author information

Authors and Affiliations

Division of Immunobiology, Institute of Immunology, Center for Pathophysiology, Infectiology and Immunology, Medical University of Vienna, Vienna, Austria
Matarr Khan, Marlis Alteneder, Moritz Madern, Monika Waldherr, Wilfried Ellmeier, Nicole Boucheron

Department of Biochemistry and Cell Biology, Max Perutz Labs, University of Vienna, Vienna BioCenter, Vienna, Austria
Wolfgang Reiter, Markus Hartl

Mass Spectrometry Core Facility, Max Perutz Labs, Vienna BioCenter, Vienna, Austria
Wolfgang Reiter, Markus Hartl

CeMM Research Center for Molecular Medicine of the Austrian Academy of Sciences, Vienna, Austria
Thomas Krausgruber, Lina Dobnikar, Christoph Bock

Institute of Artificial Intelligence, Center for Medical Data Science, Medical University of Vienna, Vienna, Austria
Thomas Krausgruber, Christoph Bock

Umeå University, the Laboratory for Molecular Infection Medicine Sweden (MIMS), Umeå Centre for Microbial Research (UCMR), Integrated Science Lab (Icelab), Department of Molecular biology, Umeå, Sweden
Johan Henriksson

Contributions

M.K. and N.B. conceptualized the study. M.K. designed, performed experiments, and analysed data including bioinformatics. M.A. contributed to all animal experiments. T.K. and L.D. contributed to the planning of scRNA-seq experiments. L.D., M.M., M.W. assisted with bioinformatics analysis. W.R. and M.H. performed quantitative mass spectrometry and data analysis. W.R., T.K., L.D., C.B., M.H., W.E. and J.H. were involved in the experiment discussions and design. J.H. performed and supervised the scRNA-seq analysis. M.K. and N.B. wrote the manuscript with contributions from all co-authors.

Corresponding author

Correspondence to Nicole Boucheron.

Ethics declarations

Competing interests

C.B. is a cofounder and scientific advisor of Myllia Biotechnology and Neurolentech. The remaining authors declare no competing interests.

Figure 1

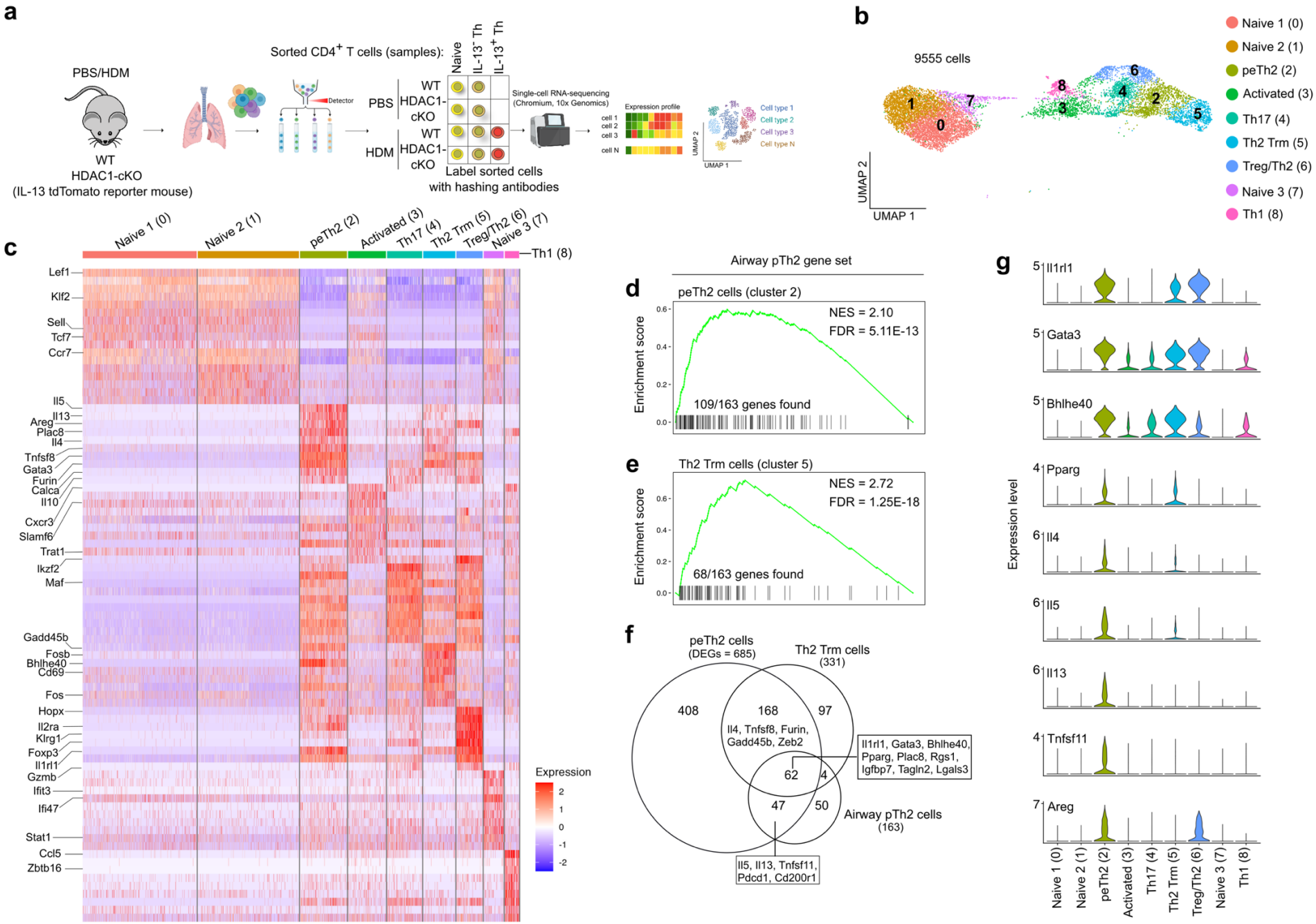
a
PBS/HDM
WT
HDAC1-cKO
(IL-13 tdTomato reporter mouse)
Detector
Sorted CD4+ T cells (samples):
Naive
IL-13- Th
IL-13+ Th
PBS
HDM
WT
HDAC1-cKO
Label sorted cells with hashing antibodies
Single-cell RNA-sequencing (Chromium, 10x Genomics)
Expression profile
cell 1
cell 2
cell 3
cell N
UMAP 2
UMAP 1
Cell type 1
Cell type 2
Cell type 3
Cell type N
b
9555 cells
UMAP 2
UMAP 1
Naive 1 (0)
Naive 2 (1)
peTh2 (2)
Activated (3)
Th17 (4)
Th2 Trm (5)
Treg/Th2 (6)
Naive 3 (7)
Th1 (8)
c
Naive 1 (0)
Naive 2 (1)
peTh2 (2)
Activated (3)
Th17 (4)
Th2 Trm (5)
Treg/Th2 (6)
Naive 3 (7)
Th1 (8)
Lef1
Klf2
Sell
Tcf7
Ccr7
Il5
Il13
Areg
Plac8
Il4
Tnfsf8
Gata3
Furin
Calca
Il10
Cxcr3
Slamf6
Trat1
Ikzf2
Maf
Gadd45b
Fosb
Bhlhe40
Cd69
Fos
Hopx
Il2ra
Klrg1
Foxp3
Il1rl1
Gzmb
Ifit3
Ifi47
Stat1
Ccl5
Zbtb16
Expression
2
1
0
-1
-2
Airway pTh2 gene set
d
peTh2 cells (cluster 2)
Enrichment score
NES = 2.10
FDR = 5.11E-13
109/163 genes found
e
Th2 Trm cells (cluster 5)
Enrichment score
NES = 2.72
FDR = 1.25E-18
68/163 genes found
f
peTh2 cells (DEGs = 685)
Th2 Trm cells (331)
Airway pTh2 cells (163)
408
168
97
62
4
47
50
Il4, Tnfsf8, Furin, Gadd45b, Zeb2
Il1rl1, Gata3, Bhlhe40, Pparg, Plac8, Rgs1, Igfbp7, Tagln2, Lgals3
Il5, Il13, Tnfsf11, Pdcd1, Cd200r1
g
Il1rl1
Gata3
Bhlhe40
Pparg
Il4
Il5
Il13
Tnfsf11
Areg
Expression level
Naive 1 (0)
Naive 2 (1)
peTh2 (2)
Activated (3)
Th17 (4)
Th2 Trm (5)
Treg/Th2 (6)
Naive 3 (7)
Th1 (8)

Fig.1| scRNA-seq analysis of lung CD4$^+$ T cells uncovers the heterogeneity of pTh2 cells in response to HDM. a, Experimental design for scRNA-seq analysis of lung CD4$^+$ T cells. After obtaining single-cell suspensions from the lungs of WT (HDAC1$^{f/f}$ x CD4-Cre$^{-/-}$) and HDAC1-cKO (HDAC1$^{f/f}$ x CD4-Cre$^{+/-}$) IL-13 tdTomato-reporter mice that were sensitised and challenged with PBS or HDM (as in Extended Data Fig. 1a), we sorted the following lung CD4$^+$ T cells: naïve (TCRβ$^+$CD4$^+$CD62L$^+$CD44$^-$IL-13$^-$), IL-13$^-$ Th (TCRβ$^+$CD4$^+$CD62L$^-$CD44$^+$IL-13$^-$), and IL-13$^+$ Th (TCRβ$^+$CD4$^+$CD62L$^-$CD44$^+$IL-13$^+$) cells. A total of ten samples based on the two genotypes (WT or HDAC1-cKO) and experimental conditions (HDM or PBS) were obtained. Each sample was labelled with a unique hashtag oligonucleotide (HTO). All ten samples were pooled for single-cell RNA-sequencing (scRNA-seq) analysis. Two independent scRNA-seq experiments were integrated for the analyses. **b**, Uniform manifold approximation and projection (UMAP) of the different lung CD4$^+$ T cell clusters identified. **c**, Heatmap shows the top 10 differentially expressed genes (DEGs) per cluster. **d-f,** Comparing the transcriptional signatures of lung peTh2 and Th2 Trm cell subsets identified in the present study to that of recently published airway pTh2 cells (Day 15 Th2 cells)[18]. **d,e,** Enrichment plots depicting the association of lung peTh2 cells (**d**) and Th2 Trm cell (**e**) with airway pTh2 cells. The list of all genes in peTh2 cells (cluster 2) and Th2 Trm cells (cluster 5) were compared with the list of DEGs (adjusted *P* value < 0.05) in the airway pTh2 gene set. **f,** Venn diagram depicting the overlap between the DEGs (adjusted *P* value < 0.05) in peTh2 and Th2 Trm cells from this study and the DEGs in the published airway pTh2 cells. **g,** Violin plots of selected marker genes associated with lung pTh2 cells. The schematic in **a** was created using BioRender. WT, wild type; HDAC1-cKO, HDAC1-conditional knockout; PBS, phosphate-buffered saline; HDM, house dust mite; Th, T helper; pTh2, pathogenic Th2; peTh2, pathogenic effector Th2, Th2 Trm, pathogenic Th2 Tissue resident memory; FDR, false discovery rate; NES, normalised enrichment score.

Figure 2

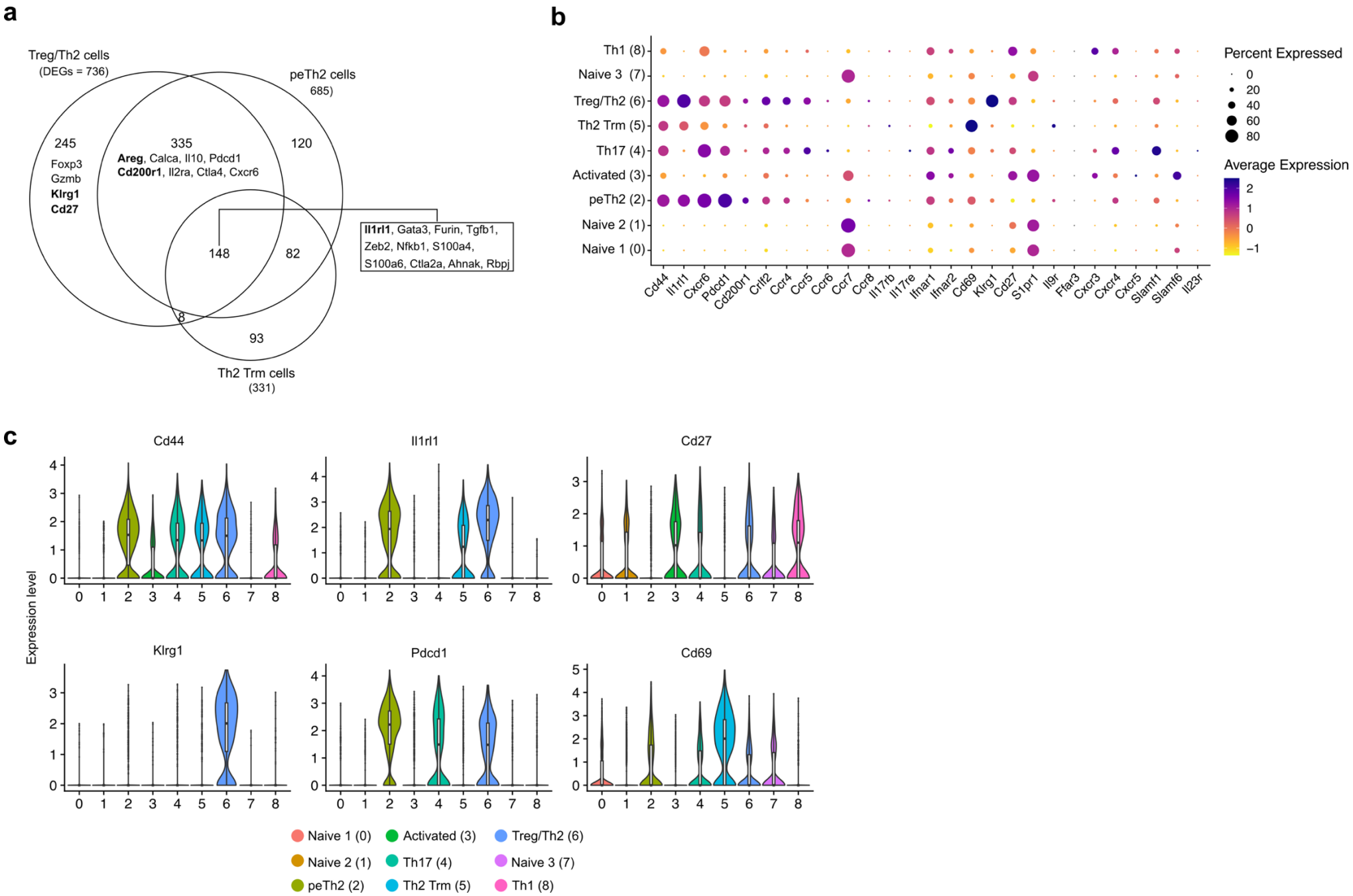
a
Treg/Th2 cells
(DEGs = 736)
peTh2 cells
685)
Th2 Trm cells
(331)
245
Foxp3
Gzmb
Klrg1
Cd27
335
Areg, Calca, Il10, Pdcd1
Cd200r1, Il2ra, Ctla4, Cxcr6
120
148
82
8
93
Il1rl1, Gata3, Furin, Tgfb1,
Zeb2, Nfkb1, S100a4,
S100a6, Ctla2a, Ahnak, Rbpj
b
Th1 (8)
Naive 3 (7)
Treg/Th2 (6)
Th2 Trm (5)
Th17 (4)
Activated (3)
peTh2 (2)
Naive 2 (1)
Naive 1 (0)
Cd44 Il1rl1 Cxcr6 Pdcd1 Cd200r1 Crlf2 Ccr4 Ccr5 Ccr6 Ccr7 Ccr8 Il17rb Il17re Ifnar1 Ifnar2 Cd69 Klrg1 Cd27 S1pr1 Il9r Ffar3 Cxcr3 Cxcr4 Cxcr5 Slamf1 Slamf6 Il23r
Percent Expressed
0
20
40
60
80
Average Expression
2
1
0
−1
c
Cd44
Il1rl1
Cd27
Klrg1
Pdcd1
Cd69
Expression level
Naive 1 (0)
Naive 2 (1)
peTh2 (2)
Activated (3)
Th17 (4)
Th2 Trm (5)
Treg/Th2 (6)
Naive 3 (7)
Th1 (8)

Fig.2| Comparison of lung ST2$^+$ Th subsets. A, Venn diagram depicting the overlapping DEGs (adjusted *P* value < 0.05) for the different lung ST2$^+$ Th subsets (peTh2, Th2 Trm, Treg/Th2, and Treg) we have identified. **B,** Dot plot showing the expression of selected genes. The size of the dot represents the percentage of cells expressing the indicated gene per cluster and the colour intensity indicates the scaled average expression level of the gene. **c,** Violin plots of selected surface markers to distinguish lung ST2$^+$ Th subsets. peTh2, pathogenic effector Th2, Th2 Trm, pathogenic Th2 Tissue-resident memory; Treg, regulatory T cell.

Figure 3

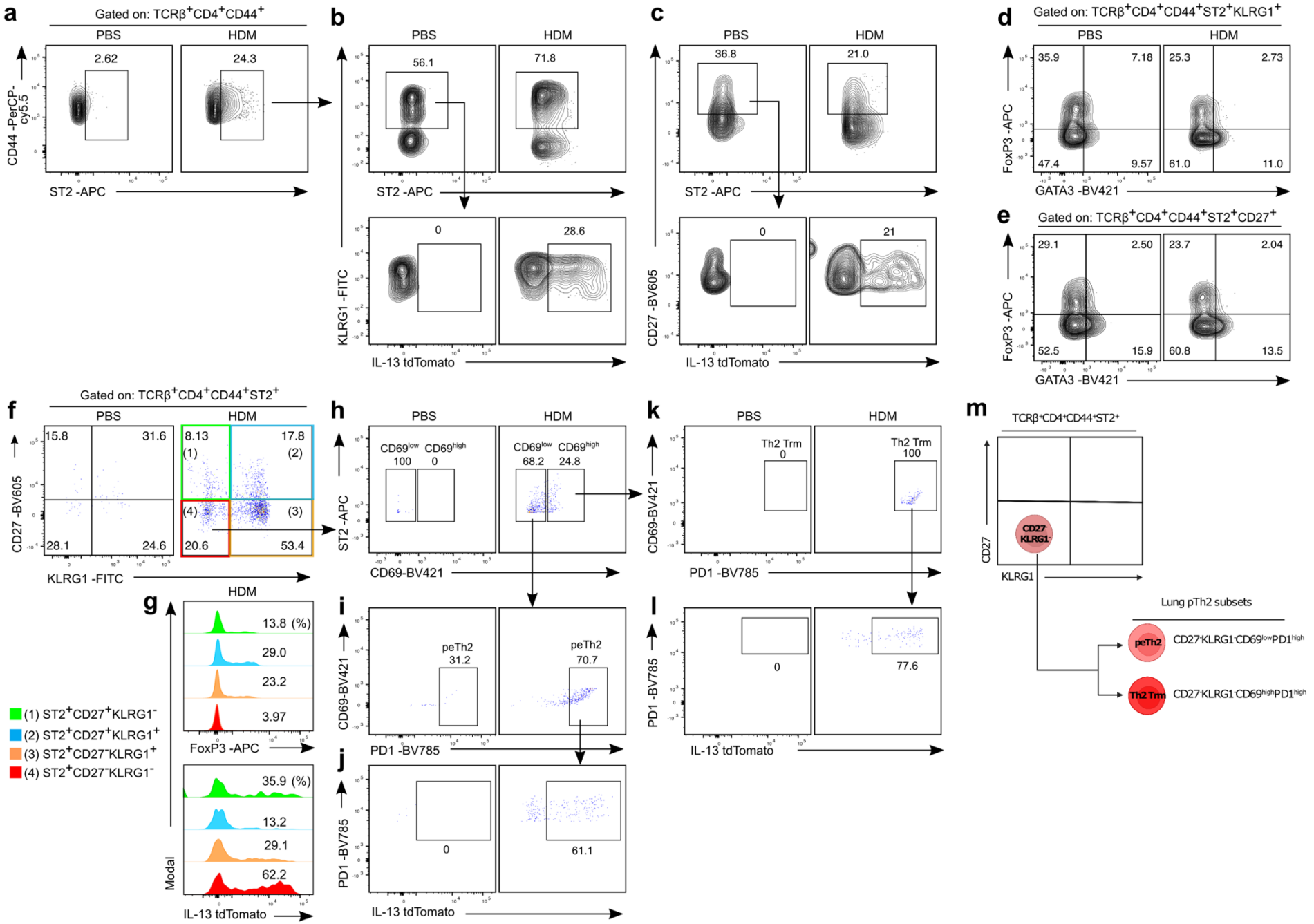
a
Gated on: TCRβ+CD4+CD44+
PBS
HDM
2.62
24.3
CD44 -PerCP-cy5.5
ST2 -APC
b
PBS
HDM
56.1
71.8
ST2 -APC
0
28.6
KLRG1 -FITC
IL-13 tdTomato
c
PBS
HDM
36.8
21.0
ST2 -APC
0
21
CD27 -BV605
IL-13 tdTomato
d
Gated on: TCRβ+CD4+CD44+ST2+KLRG1+
PBS
HDM
35.9
7.18
47.4
9.57
25.3
2.73
61.0
11.0
FoxP3 -APC
GATA3 -BV421
e
Gated on: TCRβ+CD4+CD44+ST2+CD27+
29.1
2.50
52.5
15.9
23.7
2.04
60.8
13.5
FoxP3 -APC
GATA3 -BV421
f
Gated on: TCRβ+CD4+CD44+ST2+
PBS
HDM
15.8
31.6
28.1
24.6
8.13
(1)
17.8
(2)
(4)
(3)
20.6
53.4
CD27 -BV605
KLRG1 -FITC
g
HDM
13.8 (%)
29.0
23.2
3.97
FoxP3 -APC
35.9 (%)
13.2
29.1
62.2
Modal
IL-13 tdTomato
(1) ST2+CD27+KLRG1-
(2) ST2+CD27+KLRG1+
(3) ST2+CD27-KLRG1+
(4) ST2+CD27-KLRG1-
h
PBS
HDM
CD69low CD69high
100
0
68.2
24.8
ST2 -APC
CD69-BV421
i
peTh2
31.2
peTh2
70.7
CD69-BV421
PD1 -BV785
j
0
61.1
PD1 -BV785
IL-13 tdTomato
k
PBS
HDM
Th2 Trm
0
Th2 Trm
100
CD69-BV421
PD1 -BV785
l
0
77.6
PD1 -BV785
IL-13 tdTomato
m
TCRβ+CD4+CD44+ST2+
CD27-KLRG1-
CD27
KLRG1
Lung pTh2 subsets
peTh2
CD27-KLRG1-CD69lowPD1high
Th2 Trm
CD27-KLRG1-CD69highPD1high

Fig.3| Flow cytometric characterisation of lung pTh2 subsets in response to HDM. a-l, Flow cytometry characterisation of lung $ST2^+$ Th cells in mice sensitised and challenged with PBS or HDM (as in Extended Data Fig. 1a). **a-c,** Confirmation of ST2 expression by lung $KLRG1^+$ and $CD27^+$ Th cells. **a,** Representative plots showing all lung $ST2^+$ Th cells (gated on $TCR\beta^+CD4^+CD44^+$). **b,** Representative plots showing ST2 against KLRG1 expression on Th cells gated on ST2 as depicted in **a** (top) and IL-13 expression by $ST2^+KLRG1^+$ Th cells (bottom). **c,** Representative flow cytometry plots showing ST2 against CD27 expression on Th cells gated on ST2 as depicted in **a** (top) and IL-13 expression by $ST2^+CD27^+$ Th cells (bottom). **d,** Representative plots of FoxP3 and GATA3 expression in lung Th cells (gated on $TCR\beta^+CD4^+CD44^+ST2^+KLRG1^+$). **e,** Representative plots of FoxP3 and GATA3 expression in lung Th cells (gated on $TCR\beta^+CD4^+CD44^+ST2^+CD27^+$). **f,g,** Defining the distinct subsets of lung $ST2^+$ Th cells using CD27 and KLRG1 as markers. **f,** Representative plots showing CD27 and KLRG1 expression by lung Th cells (gated on $TCR\beta^+CD4^+CD44^+ST2^+$). **g,** Histograms showing the expression of FoxP3 (top) and IL-13 (bottom) by the different $ST2^+$ Th subsets in mice exposed to HDM. **h-l,** Gating strategy to define lung peTh2 and Th2 Trm cells. **h,** Flow cytometry plots of CD69 expression ($CD69^{low}$ and $CD69^{high}$) by $CD27^-KLRG1^-$ Th cells in **f**. **i,** Flow cytometry plots showing PD1 expression by $CD69^{low}$ cells in **h**, representing peTh2 cells. **j,** IL-13 expression by peTh2 cells in **i**. **k,** Flow cytometry plots showing PD1 expression by $CD69^{high}$ cells in **h**, representing Th2 Trm cells. **l,** IL-13 expression by Th2 Trm cells in **k**. **m,** The schematic summarises the proposed surface markers to distinguish lung peTh2 cells ($TCR\beta^+CD4^+CD44^+ST2^+CD27^-KLRG1^-CD69^{low}PD1^{high}$) and Th2 Trm cells ($TCR\beta^+CD4^+CD44^+ST2^+CD27^-KLRG1^-CD69^{high}PD1^{high}$) from non-pTh2 $ST2^+$ Th cells ($ST2^+FoxP3^+$ Th cells: $ST2^+CD27^+KLRG1^-$, $ST2^+CD27^+KLRG1^+$, $ST2^+CD27^-KLRG1^+$). Data are representative of three independent experiments. The schematic in **m** was created using BioRender.

Figure 4

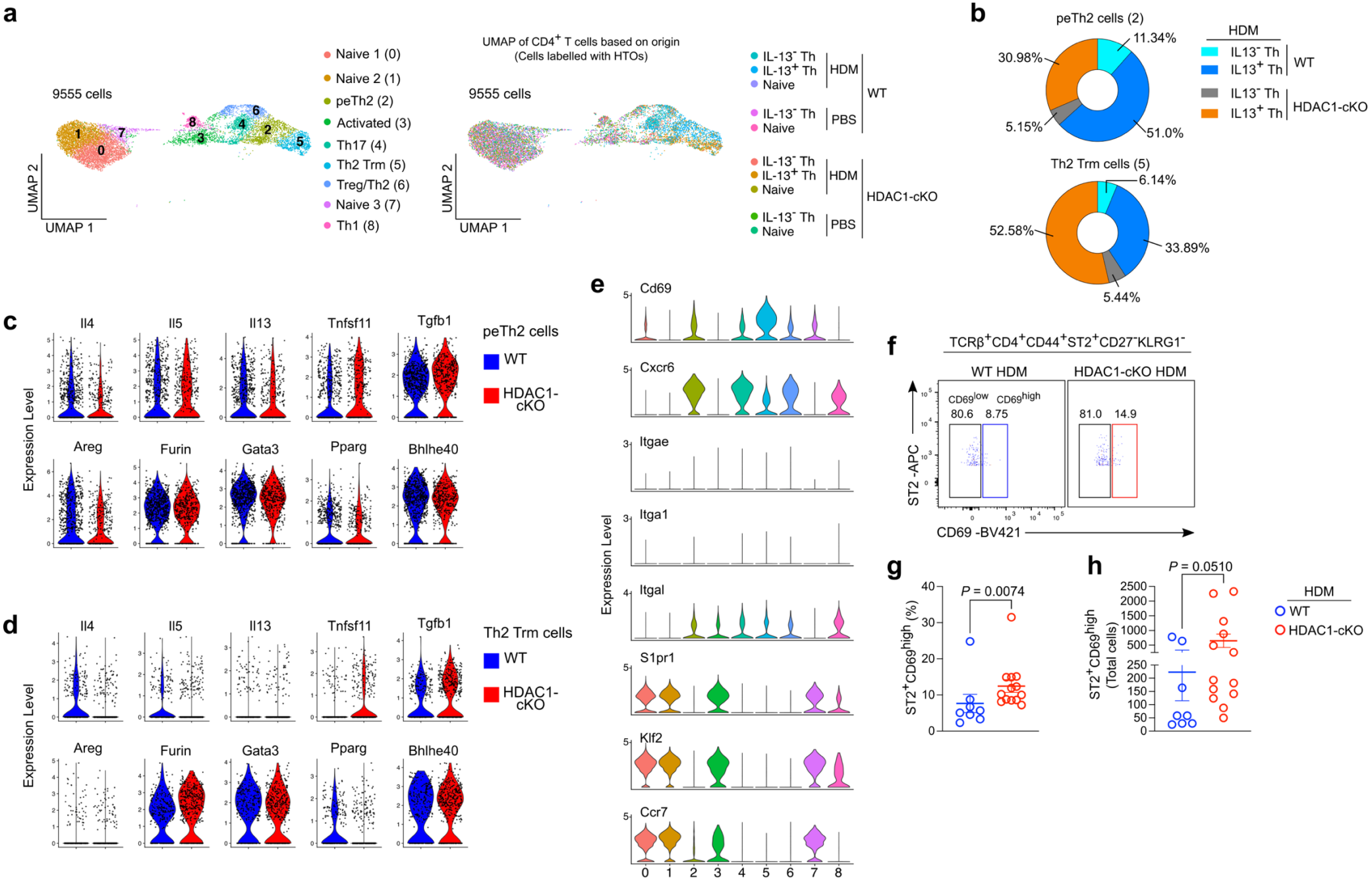
a
9555 cells
UMAP 2
UMAP 1
Naive 1 (0)
Naive 2 (1)
peTh2 (2)
Activated (3)
Th17 (4)
Th2 Trm (5)
Treg/Th2 (6)
Naive 3 (7)
Th1 (8)
UMAP of CD4+ T cells based on origin
(Cells labelled with HTOs)
9555 cells
IL-13- Th
IL-13+ Th
Naive
HDM
WT
PBS
HDAC1-cKO
b
peTh2 cells (2)
11.34%
30.98%
5.15%
51.0%
HDM
WT
HDAC1-cKO
Th2 Trm cells (5)
6.14%
52.58%
33.89%
5.44%
c
Il4
Il5
Il13
Tnfsf11
Tgfb1
Areg
Furin
Gata3
Pparg
Bhlhe40
Expression Level
peTh2 cells
WT
HDAC1-cKO
d
Th2 Trm cells
e
Cd69
Cxcr6
Itgae
Itga1
Itgal
S1pr1
Klf2
Ccr7
f
TCRβ+CD4+CD44+ST2+CD27-KLRG1-
WT HDM
HDAC1-cKO HDM
CD69low
CD69high
80.6
8.75
81.0
14.9
ST2 -APC
CD69 -BV421
g
P = 0.0074
ST2+CD69high (%)
h
P = 0.0510
ST2+CD69high (Total cells)

Fig.4| Loss of HDAC1 augments the pathogenicity of pTh2 subsets and Th2 Trm cell generation. **a,** UMAP of lung $CD4^+$ T cell clusters (left), and UMAP of lung $CD4^+$ T cell coloured by origin (sorted samples labelled with unique HTOs), representing cells from HDAC1-cKO mice exposed to either HDM or PBS, and cells from WT mice exposed to either HDM or PBS (right). **b**, Frequencies of IL-13^- Th and IL-13^+ Th cells from WT and HDAC1-cKO mice exposed to HDM in the peTh2 (top) and Th2 Trm (bottom) clusters as in **a**. **c,d,** Violin plots of selected pathogenic marker genes in peTh2 cells (**c**) and Th2 Trm cells (**d**) from WT and HDAC1-cKO mice. **e,** Violin plots of marker genes associated with tissue residency. **f,** Representative flow cytometry plots of lung $ST2^+CD69^{low}$ and $ST2^+CD69^{high}$ cells from WT and HDAC1-cKO mice sensitised and challenged to PBS or HDM. Cells in **f** are gated on $TCR\beta^+CD4^+CD44^+ST2^+CD27^-KLRG1^-$. **g,h,** Graphs show the frequency (**g**) and total number (**h**) of $ST2^+CD69^{high}$ Th cells in **f**. For **f-h,** data are pooled from three independent experiments (n = 8 for WT; n = 13 for HDAC1-cKO). For **g** and **h** data are presented as the mean ± SEM. Statistical analysis was performed using a two-tailed Mann-Whitney U test.

Figure 5

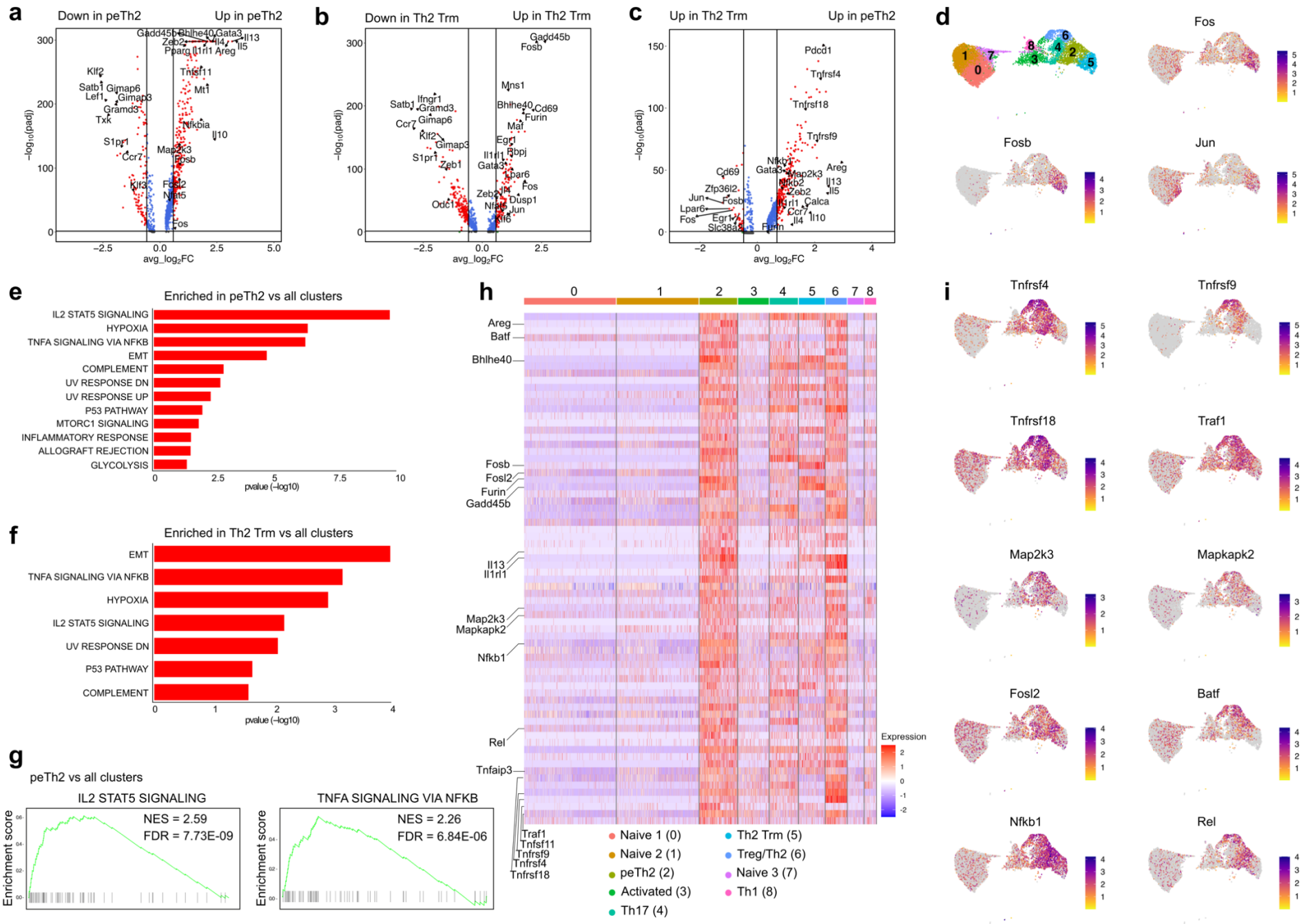
a
Down in peTh2
Up in peTh2
b
Down in Th2 Trm
Up in Th2 Trm
c
Up in Th2 Trm
Up in peTh2
avg_log2FC
−log10(padj)
d
Fos
Fosb
Jun
e
Enriched in peTh2 vs all clusters
IL2 STAT5 SIGNALING
HYPOXIA
TNFA SIGNALING VIA NFKB
EMT
COMPLEMENT
UV RESPONSE DN
UV RESPONSE UP
P53 PATHWAY
MTORC1 SIGNALING
INFLAMMATORY RESPONSE
ALLOGRAFT REJECTION
GLYCOLYSIS
pvalue (−log10)
f
Enriched in Th2 Trm vs all clusters
EMT
TNFA SIGNALING VIA NFKB
HYPOXIA
IL2 STAT5 SIGNALING
UV RESPONSE DN
P53 PATHWAY
COMPLEMENT
pvalue (−log10)
g
peTh2 vs all clusters
IL2 STAT5 SIGNALING
NES = 2.59
FDR = 7.73E-09
TNFA SIGNALING VIA NFKB
NES = 2.26
FDR = 6.84E-06
Enrichment score
h
Areg
Batf
Bhlhe40
Fosb
Fosl2
Furin
Gadd45b
Il13
Il1rl1
Map2k3
Mapkapk2
Nfkb1
Rel
Tnfaip3
Traf1
Tnfsf11
Tnfrsf9
Tnfrsf4
Tnfrsf18
Expression
Naive 1 (0)
Naive 2 (1)
peTh2 (2)
Activated (3)
Th17 (4)
Th2 Trm (5)
Treg/Th2 (6)
Naive 3 (7)
Th1 (8)
i
Tnfrsf4
Tnfrsf9
Tnfrsf18
Traf1
Map2k3
Mapkapk2
Fosl2
Batf
Nfkb1
Rel

Fig.5| Lung pTh2 subsets exhibit shared and distinct transcriptional signatures. a-c, Volcano plots showing a comparison between peTh2 cells and all other clusters (**a**), Th2 Trm cells and all other clusters (**b**), and peTh2 cells and Th2 Trm cells (**c**). The vertical and horizontal lines indicate fold change ≥ 1.5 and adjusted *P* value < 0.05, respectively. **d,** UMAP plots of $CD4^+$ T cells colour-coded based on the log-normalised expression levels of selected genes. **e,** GSEA of HALLMARK pathways upregulated (*P* value < 0.05) in peTh2 cells as compared with all other clusters. **f,** GSEA of HALLMARK pathways upregulated (*P* value < 0.05) in Th2 Trm cells as compared with all other clusters. **g,** Enrichment plots of the IL-2/STAT5 (top) and TNFA/NFκB (bottom) pathways in peTh2 cells (Fig. 5e). **h,** Heatmap shows the leading-edge genes for the pathways in **g. i,** UMAP plots of $CD4^+$ T cells colour-coded based on the log-normalised expression levels of selected genes. IL-2, Interleukin-2; STAT5, signal transducer and activator of transcription factor 5; TNFA, tumour necrosis factor alpha; NFKB, nuclear factor kappa B; EMT, epithelial-mesenchymal transition; UV, ultraviolet; FDR, false discovery rate; NES, normalised enrichment score.

Figure 6

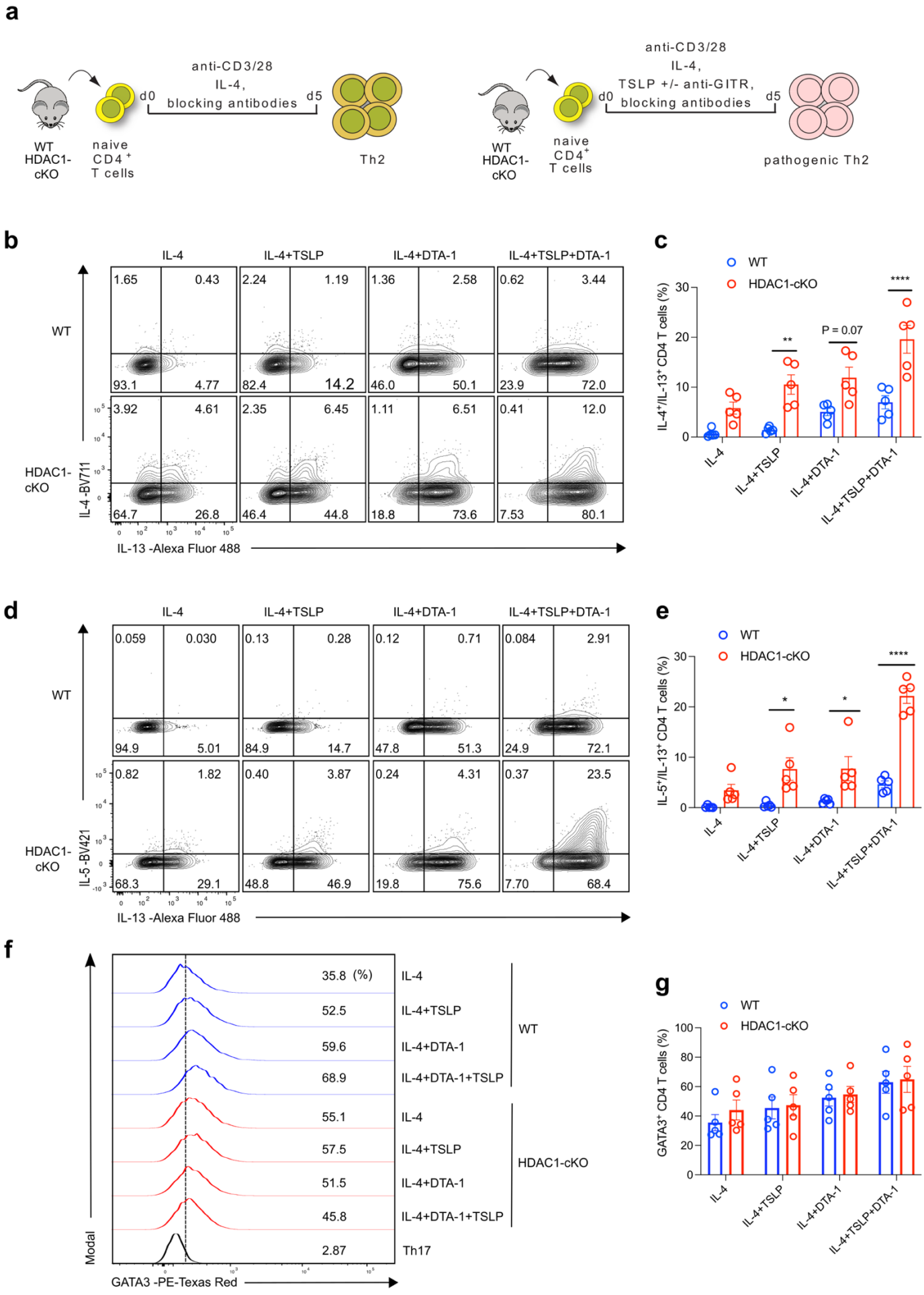

Fig.6| Co-stimulation of GITR and TSLPR drives *in vitro* differentiation of pTh2 cells. a, Schematic of *in vitro* differentiation of Th2 cells (left) and pTh2 cells (right). Naïve $CD4^+$ T cells ($TCR\beta^+CD4^+CD62L^+CD44^-$) from WT and HDAC1-cKO mice were activated with anti-CD3 and anti-CD28 in the presence of Th2-promoting conditions (IL-4, IL-2, anti-IFN-γ, and anti-TGF-β; collectively referred as IL-4), or Th2-promoting conditions plus TSLP alone, anti-GITR antibody (DTA-1) alone, or both TSLP and DTA-1, then cultured for 5 days. On day 5, cells were restimulated with PMA and ionomycin in the presence of GolgiStop and GolgiPlug for 4 hours, and cytokine analyses were performed by flow cytometry. **b-g,** Flow cytometric analysis of cells differentiated under conditions indicated in **a**. **b,** Representative plots showing the expression of IL-4 and IL-13 in WT cells (top) and HDAC1-cKO cells (bottom). **c,** Graph shows the frequency of IL-4 and IL-13 co-expressing cells in **b**. **d,** Representative plots showing the expression of IL-5 and IL-13 in WT cells (top) and HDAC1-cKO cells (bottom). **e,** Graph shows the frequency of IL-5 and IL-13 co-expressing cells in **d**. **f,** Histograms depicting the expression of GATA3 in WT cells (blue) and HDAC1-cKO cells (red). Th17 cells were used as controls for gating. **g,** Graph shows the frequency of GATA3 expressing cells in **f.** Data are pooled from five independent experiments and presented as the mean ± SEM. Each symbol represents one mouse. Statistical analysis was performed using a Two-way ANOVA with Tukey's multiple comparisons test. $^{*}P<0.05$, $^{**}P<0.01$, $^{****}P<0.0001$. The schematics in **a** were created using BioRender. TSLP, thymic stromal lymphopoietin; GITR, glucocorticoid-induced TNFR-related protein.

Figure 7

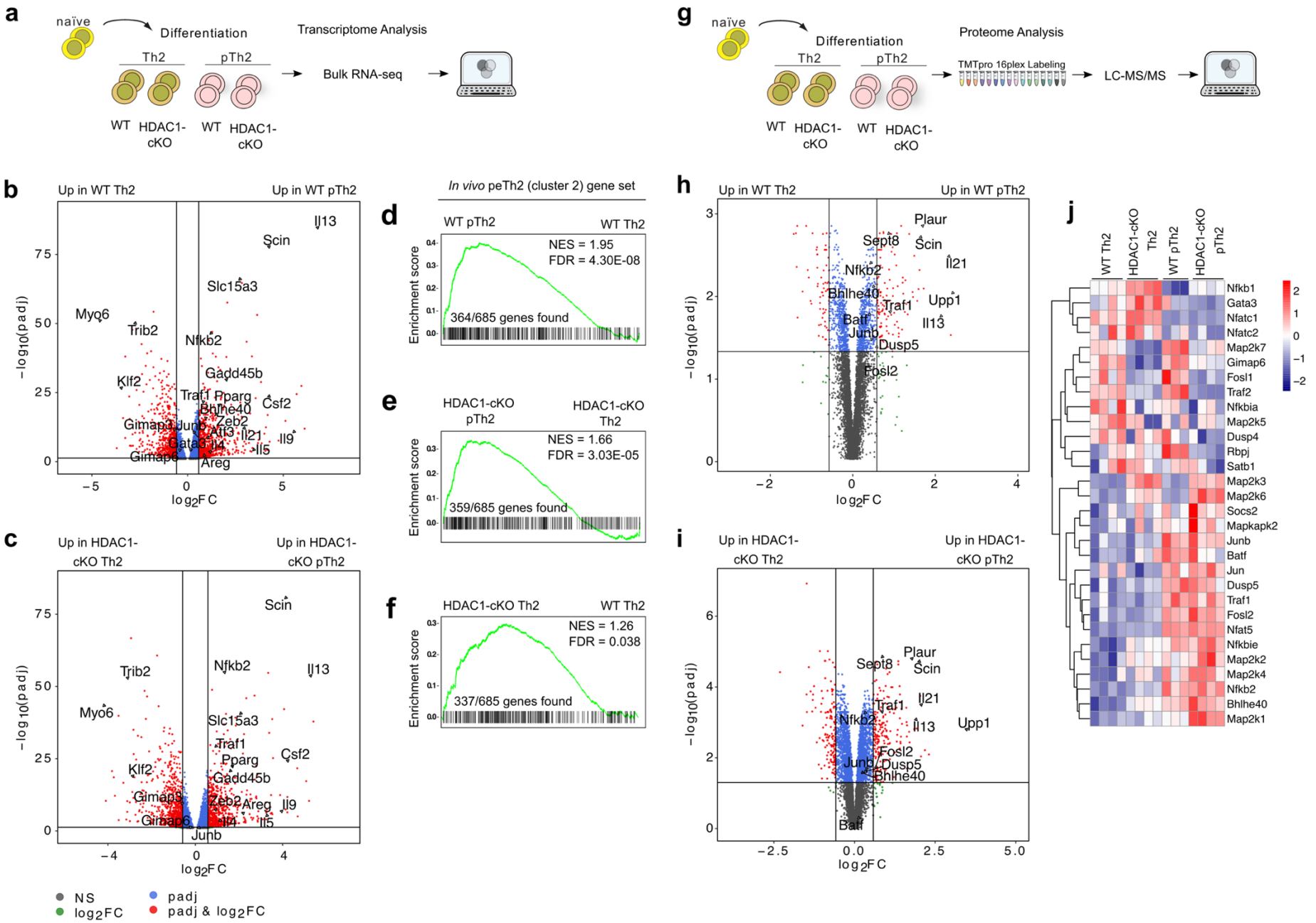
a
naïve
Differentiation
Th2
pTh2
WT
HDAC1-cKO
WT
HDAC1-cKO
Transcriptome Analysis
Bulk RNA-seq
g
naïve
Differentiation
Th2
pTh2
WT
HDAC1-cKO
WT
HDAC1-cKO
Proteome Analysis
TMTpro 16plex Labeling
LC-MS/MS
b
Up in WT Th2
Up in WT pTh2
−log10(padj)
log2FC
Il13
Scin
Slc15a3
Myo6
Trib2
Nfkb2
Gadd45b
Klf2
Traf1
Pparg
Bhlhe40
Csf2
Zeb2
Atf3
Il21
Il9
Gata3
Il4
Il5
Gimap3
Jun
Gimap6
Areg
c
Up in HDAC1-cKO Th2
Up in HDAC1-cKO pTh2
−log10(padj)
log2FC
Scin
Trib2
Nfkb2
Il13
Myo6
Slc15a3
Traf1
Pparg
Csf2
Klf2
Gadd45b
Gimap3
Zeb2
Areg
Il9
Gimap6
Il4
Il5
Junb
NS
log2FC
padj
padj & log2FC
d
In vivo peTh2 (cluster 2) gene set
WT pTh2
WT Th2
Enrichment score
NES = 1.95
FDR = 4.30E-08
364/685 genes found
e
HDAC1-cKO pTh2
HDAC1-cKO Th2
Enrichment score
NES = 1.66
FDR = 3.03E-05
359/685 genes found
f
HDAC1-cKO Th2
WT Th2
Enrichment score
NES = 1.26
FDR = 0.038
337/685 genes found
h
Up in WT Th2
Up in WT pTh2
−log10(padj)
log2FC
Plaur
Sept8
Scin
Il21
Nfkb2
Bhlhe40
Upp1
Traf1
Batf
Il13
Junb
Dusp5
Fosl2
i
Up in HDAC1-cKO Th2
Up in HDAC1-cKO pTh2
−log10(padj)
log2FC
Plaur
Sept8
Scin
Traf1
Il21
Nfkb2
Il13
Upp1
Fosl2
Junb
Dusp5
Bhlhe40
Batf
j
WT Th2
HDAC1-cKO Th2
WT pTh2
HDAC1-cKO pTh2
Nfkb1
Gata3
Nfatc1
Nfatc2
Map2k7
Gimap6
Fosl1
Traf2
Nfkbia
Map2k5
Dusp4
Rbpj
Satb1
Map2k3
Map2k6
Socs2
Mapkapk2
Junb
Batf
Jun
Dusp5
Traf1
Fosl2
Nfat5
Nfkbie
Map2k2
Map2k4
Nfkb2
Bhlhe40
Map2k1
2
1
0
−1
−2

Fig.7| Combined transcriptome and proteome profiling reveals a shared signature between *in vitro* generated pTh2 and lung peTh2 cells. a, Schematic of Bulk RNA-seq of *in vitro* generated Th2 cells (IL-4, IL-2, anti-IFN-γ, and anti-TGF-β) and pTh2 cells (IL-4, IL-2, TSLP, DTA-1, anti-IFN-γ, and anti-TGF-β) from WT and HDAC1-cKO. Th2 and pTh2 cells were cultured for 72 hours, then harvested and prepared for transcriptome profiling. **b,** Volcano plot of DEGs between WT pTh2 cells and WT Th2 cells. **c,** Volcano plot of DEGs between HDAC1-cKO pTh2 cells and HDAC1-cKO Th2 cells. **d-f,** GSEA of *in vitro* generated pTh2 cells to lung peTh2 cells. **d,** Enrichment plot showing a comparison of WT pTh2 cells and WT Th2 cells to lung peTh2 cells. **e,** Enrichment plot showing comparison of HDAC1-cKO pTh2 cells and HDAC1-cKO Th2 cells to lung peTh2 cells. **f,** Enrichment plot showing comparison of HDAC1-cKO Th2 cells and WT Th2 cells to lung peTh2 cells. Significant gene lists (adjusted *P* value < 0.01) between WT pTh2 vs WT Th2, HDAC1-cKO pTh2 vs HDAC1-cKO Th2, and HDAC1-cKO Th2 vs WT Th2 (obtained by DESeq2 analysis; Supplementary Table 7) were used to compare with lung peTh2 gene set (DEGs; adjusted *P* value < 0.05; Supplementary Table 2). **g,** Schematic of proteomics analysis of *in vitro* generated Th2 and pTh2 cells from WT and HDAC1-cKO as in **a**. The cells were cultured for 72 hours, harvested, and prepared for proteome profiling. **h,i,** Volcano plots depicting proteomics comparison between WT pTh2 and WT Th2 cells (**h)** and HDAC1-cKO pTh2 and HDAC1-cKO Th2 cells (**i**). **j,** Heatmap showing normalised reporter ion intensity values of selected proteins. For **b,c,h,i,** the vertical and horizontal lines indicate Fold Change ≥ 1.5 and adjusted *P* value < 0.05, respectively. Transcriptomic and proteomic data are from three and four independent experiments, respectively. One WT pTh2 sample was excluded from the proteomics analyses due to poor sample quality.

Figure 8

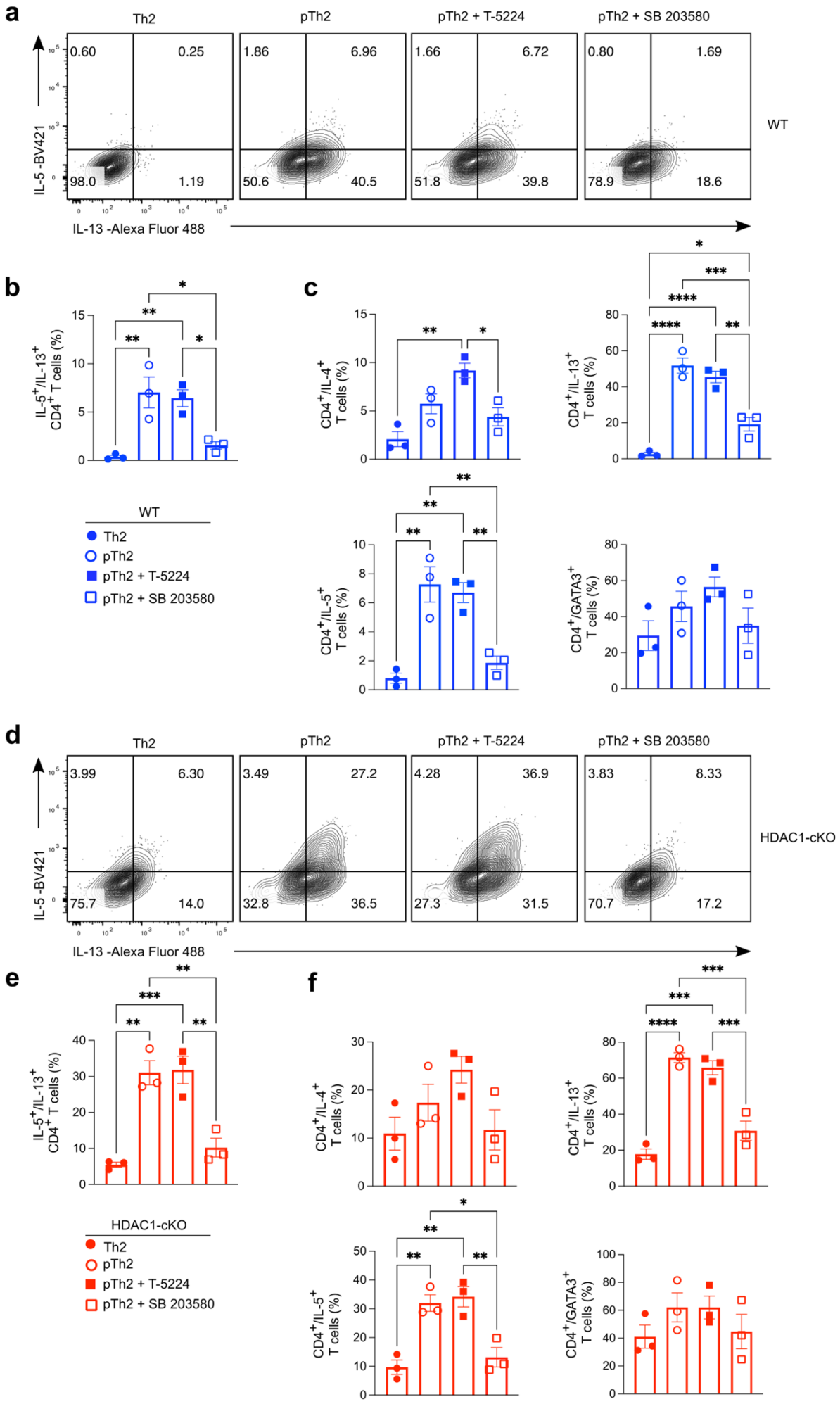

Fig.8| The p38 MAPK pathway regulates IL-5 and IL-13 expression in pTh2 cells. a-f, Impact of targeting AP-1 or p38 MAPK pathways on pTh2 cells generated *in vitro*. Th2 cells alone, pTh2 cells alone, pTh2 cells treated with an AP-1 inhibitor (T-5224; 10 μM), and pTh2 cells treated with a p38 MAPK inhibitor (SB 203580; 10 μM) were cultured for five days under Th2 and pTh2-promoting conditions (Fig. 7a). On day 5, cells were restimulated with PMA and ionomycin in the presence of GolgiStop and GolgiPlug for 4 hours before cytokine analyses by flow cytometry. **a-c,** Flow cytometric analysis of WT cells. **a,** Representative flow cytometry plots showing IL-5 and IL-13 expression under indicated conditions. **b,** Graph shows the frequency of IL-5 and IL-13 co-expressing cells in **a**. **c,** Graphs showing the frequencies of IL-4, IL-5, IL-13, and GATA3 single-expressing cells. **d-f,** Flow cytometric analysis of HDAC1-cKO cells. **d,** Representative flow cytometry plots showing IL-5 and IL-13 co-expression. **e,** Graph shows the frequency of IL-5 and IL-13 co-expressing cells in **d**. **f,** Graphs showing frequencies of IL-4, IL-5, IL-13, and GATA3 single-expressing cells. Data are pooled from three independent experiments and presented as the mean ± SEM. Each symbol represents one mouse. Statistical analysis was performed using a one-way ANOVA with Tukey's multiple comparisons test. $^{*}P<0.05$, $^{**}P<0.01$, $^{***}P<0.001$, $^{****}P<0.0001$. AP-1, activator protein-1; p38 MAPK, p38 mitogen-activated protein kinase.

Extended Data Figure 1

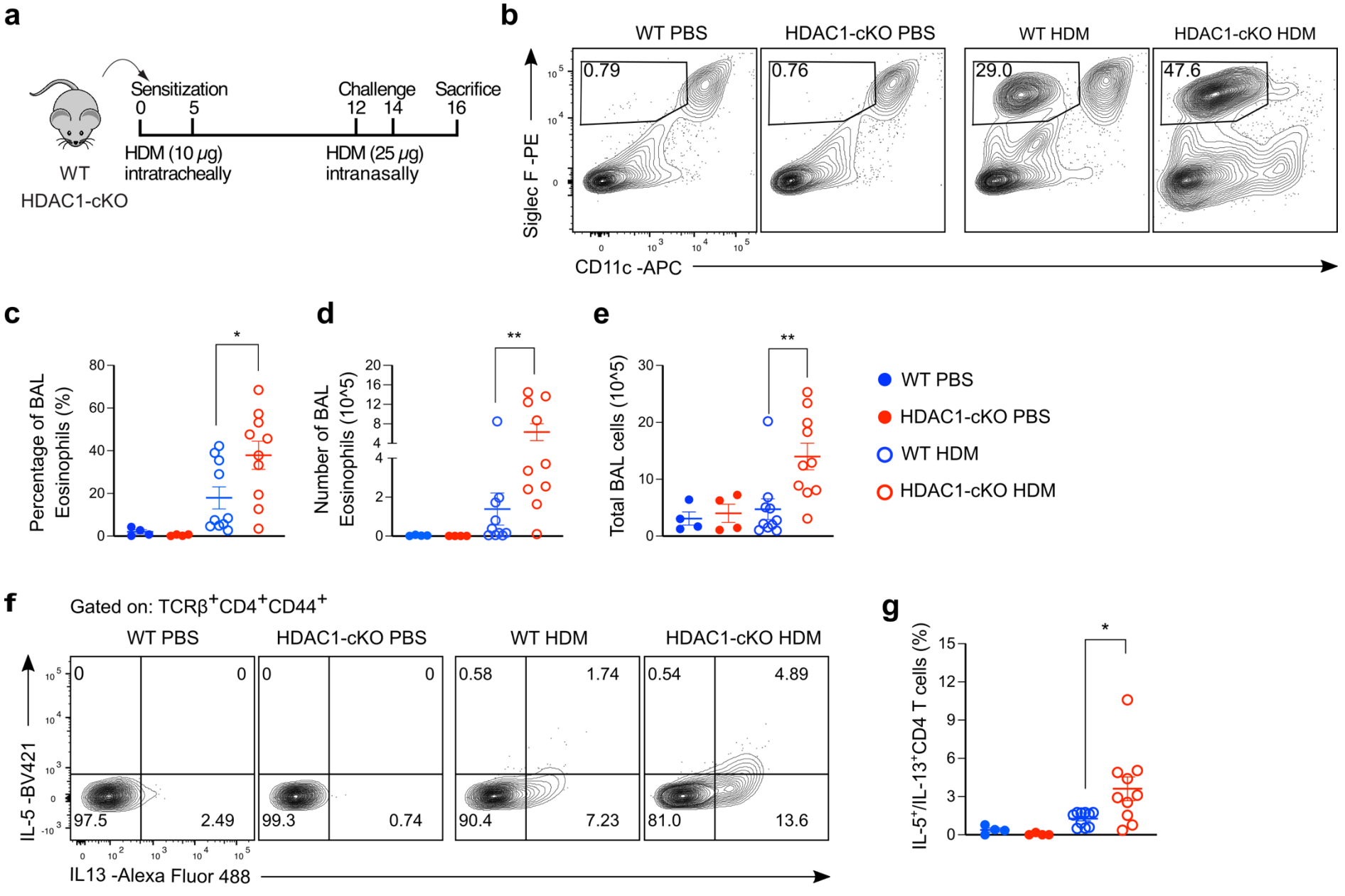

Extended Data Fig.1| HDAC1 is essential to restrict HDM-induced airway inflammation. a, Model of HDM-induced allergic airway inflammation. WT (HDAC1$^{f/f}$ x CD4-Cre$^{-/-}$) and HDAC1-cKO (HDAC1$^{f/f}$ x CD4-Cre$^{+/-}$) mice were sensitised with 10 µg HDM in 40 µl PBS on days 0 and 5. The mice were challenged on days 12 and 14 with 25 µg HDM in 40 µl PBS and euthanised on day 16. Control mice received 40 µl PBS alone during the sensitisation and challenge periods. **b,** Representative flow cytometry plots showing eosinophils (Siglec F^{+}CD11c^{-}) in BAL of the mice with the indicated genotype. **c,** Graph shows the frequency of eosinophils in **b**. **d,e,** Graphs showing the summary of total number of BAL eosinophils (**d**) and the total number of cells in BAL (**e**). **f,g,** *Ex vivo* restimulation of lung cells from WT and HDAC1-cKO control and diseased mice. Lung cells were restimulated with PMA and ionomycin in the presence of GolgiStop and GolgiPlug for 4 hours followed by cytokine analyses by flow cytometry. **f,** Representative flow cytometry plots showing IL-5 and IL-13 expression in lung Th cells (gated on TCRβ^{+}CD4^{+}CD44^{+}). **g,** Graph shows the frequency of IL-5 and IL-13 co-expressing cells in **f.** Data are pooled from two independent experiments (PBS groups: n = 4; HDM groups: n = 10) with each symbol representing one mouse. Data are presented as the mean ± SEM and statistical analysis was performed using a two-tailed Mann-Whitney U test. $^{*}P$<0.05, $^{**}P$<0.01. WT, wild type; HDAC1-cKO, HDAC1-conditional knockout; PBS, phosphate-buffered saline; HDM, house dust mite; BAL, bronchoalveolar lavage; PMA, phorbol 12-myristate 13-acetate; Th, T helper.

Extended Data Figure 2

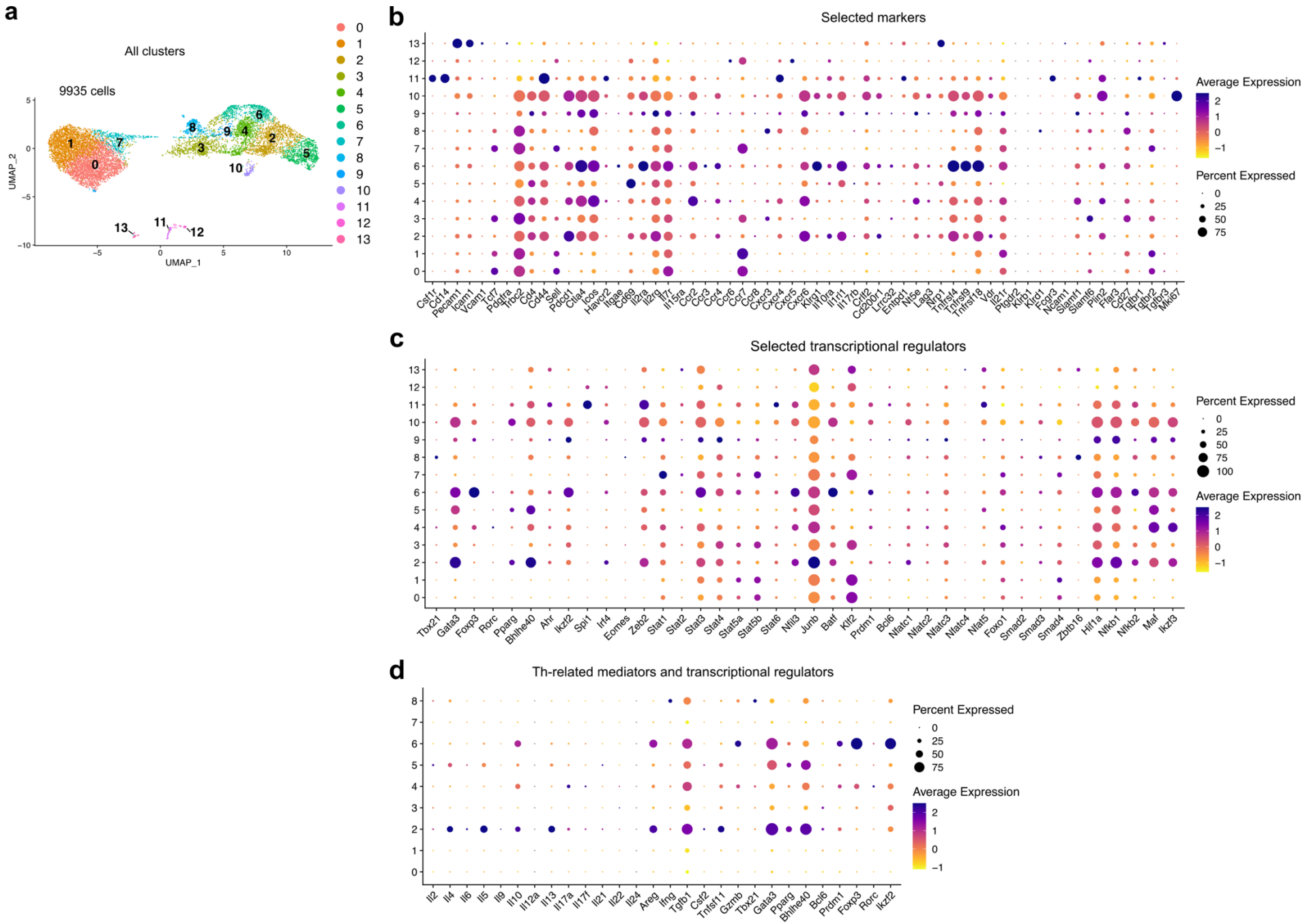

Extended Data Fig.2| Selected markers, transcriptional regulators, and mediators. a-d, scRNA-seq analysis of lung $CD4^+$ T cells in response to PBS or HDM. **a,** UMAP showing all fourteen lung $CD4^+$ T cell clusters identified. **b-d,** Defining the identity of the clusters in **a**. Dot plots showing the expression of selected markers (**b**), transcriptional regulators (**c**), and Th-related mediators and transcription factors (**d**). The size of each dot denotes the percentage of cells expressing the indicated gene for each cluster and the colour intensity of the dot represents the expression level of the gene.

Extended Data Figure 3

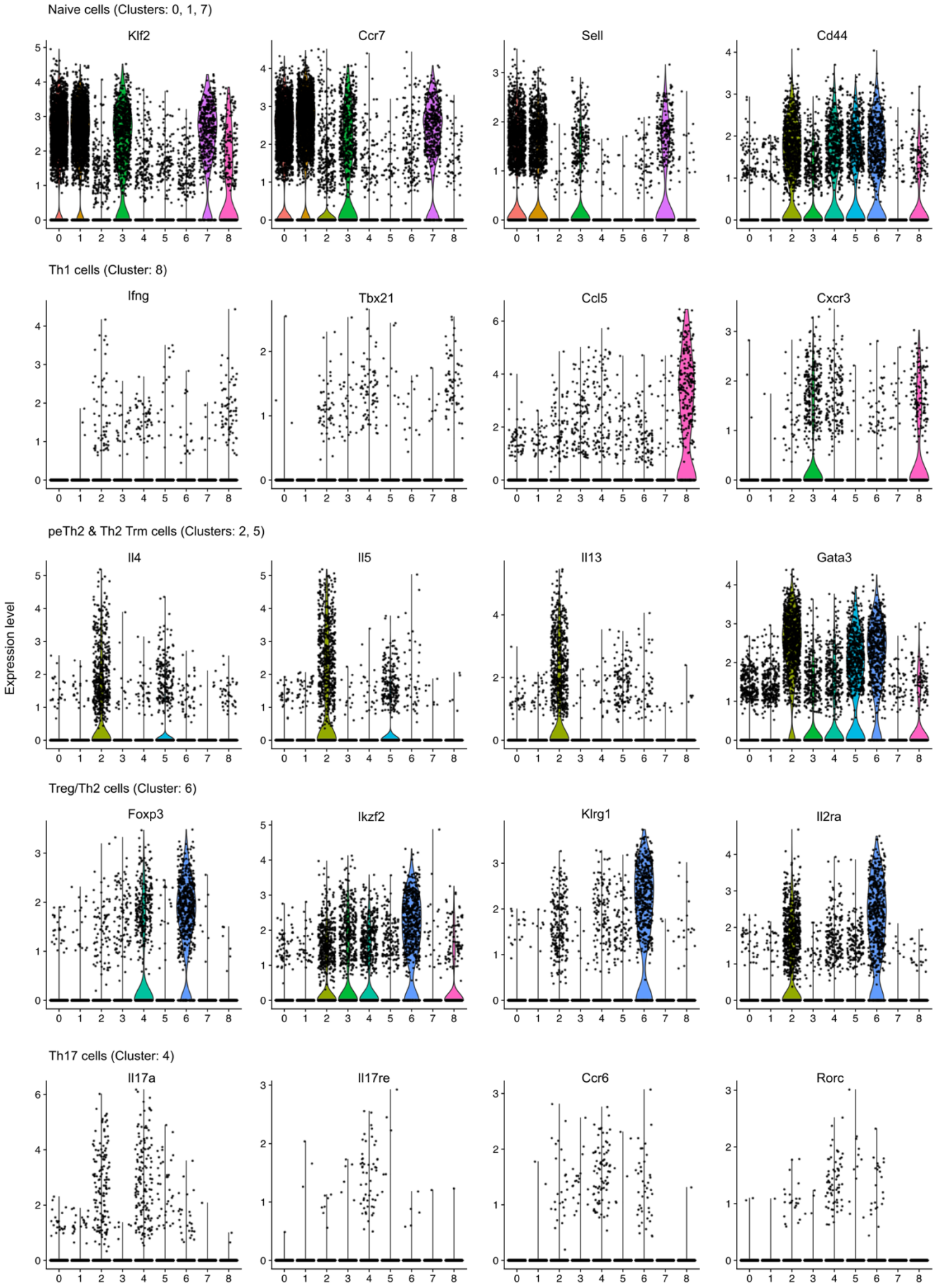

Extended Data Fig.3| Th lineage-specific markers and comparison of pTh2 cell subsets to published data obtained from airway pTh2 cell scRNAseq. Violin plots of selected genes expressed by naïve $CD4^+$ T cells and Th-lineages.

Extended Data Figure 4

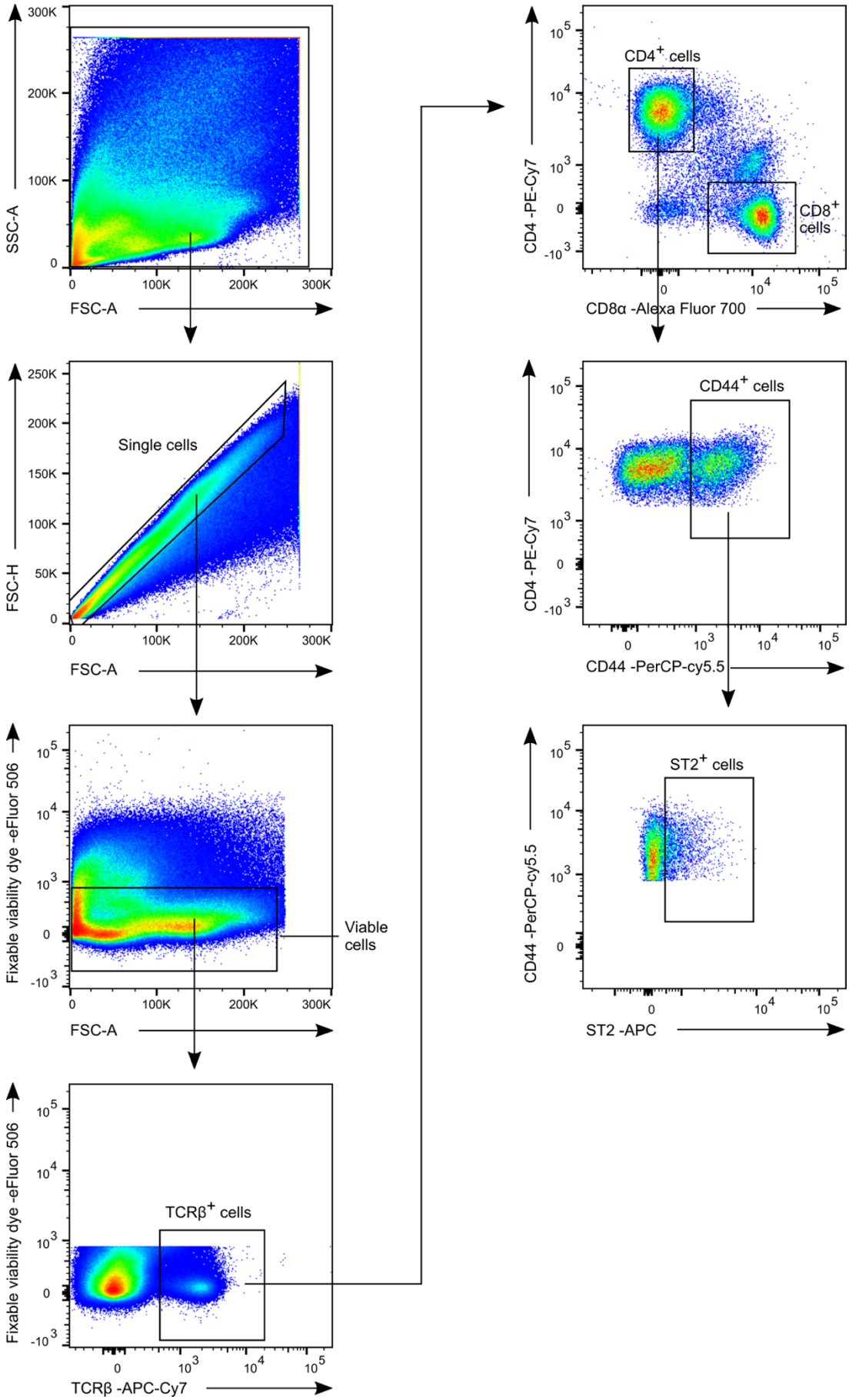

Extended Data Fig.4| Gating strategy for lung ST2$^+$ Th cells. Representative flow cytometry plots showing the gating strategy for lung Th cells. The plots shown are from a WT mouse sensitised and challenged with HDM (as in Extended Data Fig. 1a). Single cells were obtained by gating away all the doublet cells. Next, we gated on the viable cells by excluding all dead cells from the single cells using a fixable viability dye. We then identified the T cells by gating on TCRβ$^+$ cells. CD4$^+$ T cells and cytotoxic CD8$^+$ T cells in the TCRβ$^+$ population were identified based on the expression of CD4 and CD8α, respectively. CD44 was used to exclude naïve CD4$^+$ T cells and mark all Th (effector) cells within the CD4$^+$ T cells. And all ST2$^+$ cells were gated on the CD44$^+$ cells.

Extended Data Figure 5

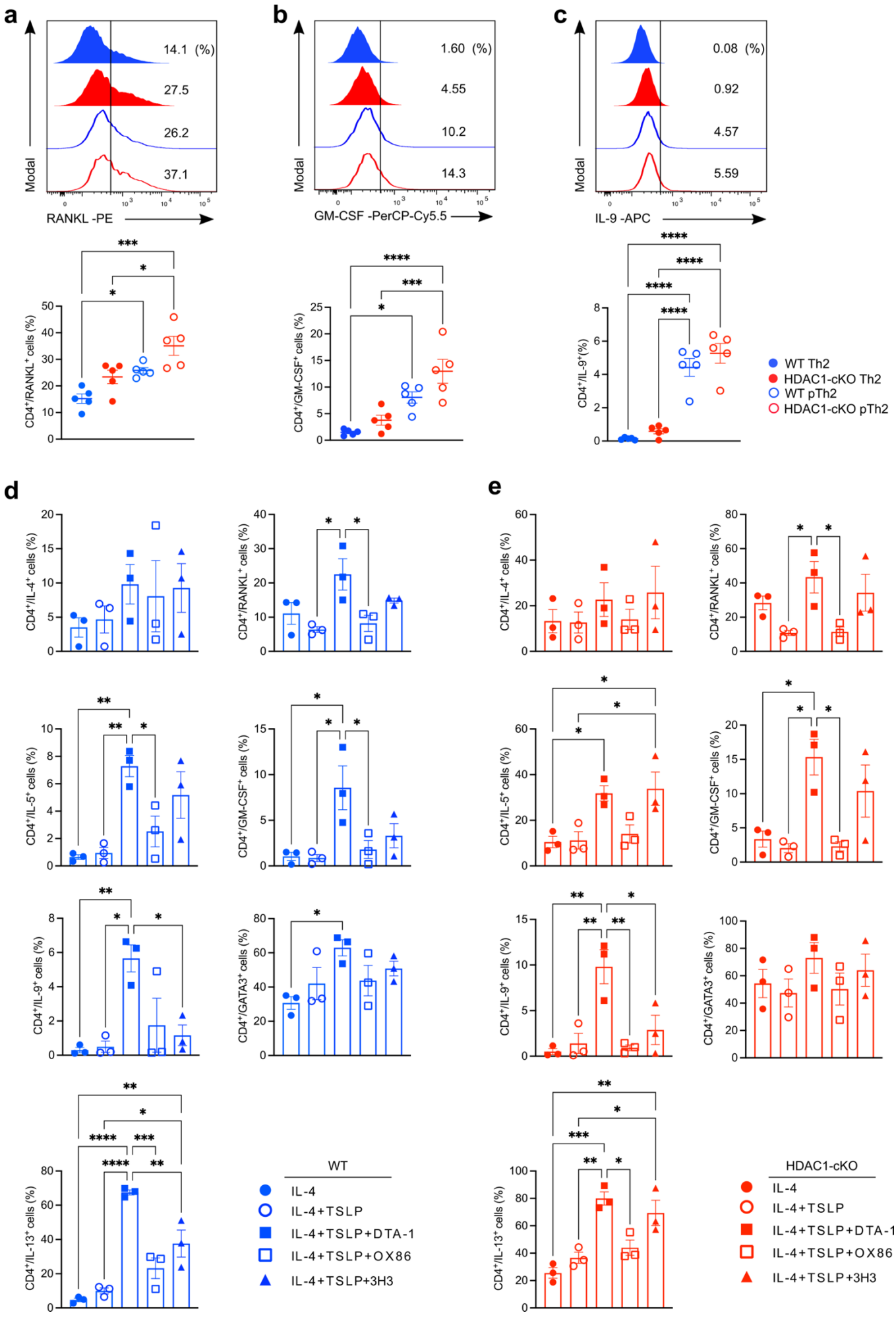

Extended Data Fig.5| Flow cytometric analysis of pathogenic mediators and comparison of TNFRSF members. a-c, Analyses of pathogenic mediators in *in vitro* generated pTh2 cells. Naïve $CD4^+$ T cells ($TCR\beta^+CD4^+CD62L^+CD44^-$) from WT and HDAC1-cKO mice were activated with anti-CD3 and anti-CD28 in the presence of Th2-promoting conditions (IL-4, IL-2, anti-IFN-γ, and anti-TGF-β) or pTh2-promoting conditions (IL-4, IL-2, TSLP, DTA-1, anti-IFN-γ, and anti-TGF-β) and cultured for 5 days. On day 5, we restimulated the cells with PMA and ionomycin in the presence of GolgiStop and GolgiPlug for 4 hours and performed cytokine analyses by flow cytometry. **a,** Histogram shows the expression of RANKL (top) and the frequency of Th cells expressing RANKL (bottom). **b,** Histogram shows the expression of GM-CSF (top) and the frequency of Th cells expressing GM-CSF (bottom). **c,** Histogram shows the expression of IL-9 (top) and the frequency of Th cells expressing IL-9 (bottom). **d,e,** Comparing the impact of TNFRSF members in inducing a pathogenic program in Th2 cells. We isolated naïve $CD4^+$ T cells ($TCR\beta^+CD4^+CD62L^+CD44^-$) from WT and HDAC1-cKO mice and activated them with anti-CD3 and anti-CD28 in the presence of Th2-promoting conditions (IL-4, IL-2, anti-IFN-γ, and anti-TGF-β; collectively termed IL-4), or IL-4+TSLP alone, or IL-4+TSLP+DTA-1, or IL-4+TSLP+OX86, or IL-4+TSLP+3H3. We cultured the cells for 5 days and restimulated them with PMA and ionomycin in the presence of GolgiStop and GolgiPlug for 4 hours before cytokine analyses by flow cytometry. **d,** Graphs showing the frequencies of pathogenic Th2 mediators and GATA3 in WT cells (blue). **e,** Graphs showing the frequencies of pathogenic Th2 mediators and GATA3 in HDAC1-cKO cells (red). Data are pooled from three independent experiments and presented as the mean ± SEM. Each symbol represents one mouse. Statistical analysis was performed using a one-way ANOVA with Tukey's multiple comparisons test. $^*P<0.05$, $^{**}P<0.01$, $^{***}P<0.001$, $^{****}P<0.0001$. TSLP, thymic stromal lymphopoietin; DTA-1, agonistic antibody against GITR (TNFRSF18); OX86, agonistic antibody against OX40 (TNFRSF4); 3H3, agonistic antibody against 4-1BB (TNFRSF9).

Extended Data Figure 6

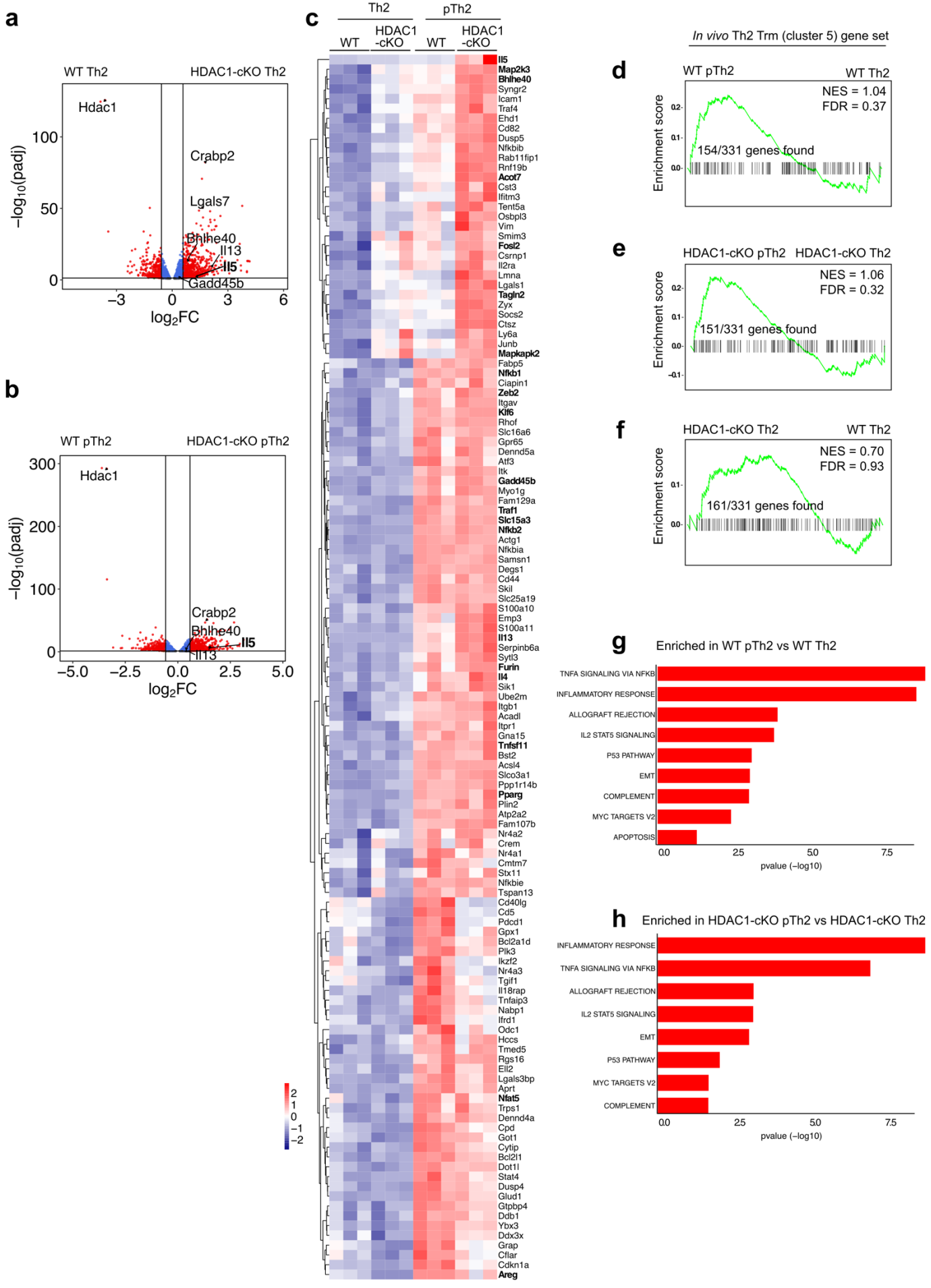

Extended Data Fig.6| Transcriptomic analysis of *in vitro* generated pTh2 cells. a-f, Transcriptome profiling of *in vitro* differentiated Th2 and pTh2 cells. Naïve $CD4^+$ T cells from WT and HDAC1-cKO mice were differentiated under Th2-promoting conditions (IL-4, IL-2, anti-IFN-γ, and anti-TGF-β) and pTh2-promoting conditions (IL-4, IL-2, TSLP, DTA-1, anti-IFN-γ, and anti-TGF-β) for 72 hours, then harvested and prepared for transcriptome profiling. **a,b,** Volcano plots showing comparison between WT Th2 and HDAC1-cKO Th2 (**a**) and WT pTh2 and HDAC1-cKO pTh2 (**b**). The vertical and horizontal lines indicate Fold Change ≥ 1.5 and adjusted *P* value < 0.05, respectively. **c,** Heatmap showing the expression profiles of WT pTh2 leading-edge genes (Fig. 7d) across *in vitro* differentiated Th2 and pTh2 cells from WT and HDAC1-cKO mice. The heatmap was generated using the DESeq2 normalised counts of the leading-edge genes (Supplementary Table 9). **d,** Enrichment plot showing a comparison of WT pTh2 cells and WT Th2 cells to lung Th2 Trm cells. **e,** Enrichment plot showing comparison of HDAC1-cKO pTh2 cells and HDAC1-cKO Th2 cells to lung Th2 Trm cells. **f,** Enrichment plot showing a comparison of HDAC1-cKO Th2 cells and WT Th2 cells to lung Th2 Trm cells. Significant gene lists (adjusted *P* value < 0.01) between WT pTh2 vs WT Th2, HDAC1-cKO pTh2 vs HDAC1-cKO Th2, and HDAC1-cKO Th2 vs WT Th2 (obtained by DESeq2 analysis; Supplementary Table 7) were used to compare with lung Th2 Trm gene set (DEGs; adjusted *P* value < 0.05; Supplementary Table 2). **g,** GSEA of HALLMARK pathways upregulated (*P* value < 0.05) in *in vitro* generated WT pTh2 vs WT Th2. **h,** GSEA of HALLMARK pathways upregulated (*P* value < 0.05) in *in vitro* generated HDAC1-cKO pTh2 vs HDAC1-cKO Th2. Transcriptomic data are from three independent experiments. TNFA, tumour necrosis factor alpha; NFKB, nuclear factor kappa B; IL-2, Interleukin-2; STAT5, signal transducer and activator of transcription factor 5; EMT, epithelial-mesenchymal transition; FDR, false discovery rate; NES, normalised enrichment score.

Extended Data Figure 7

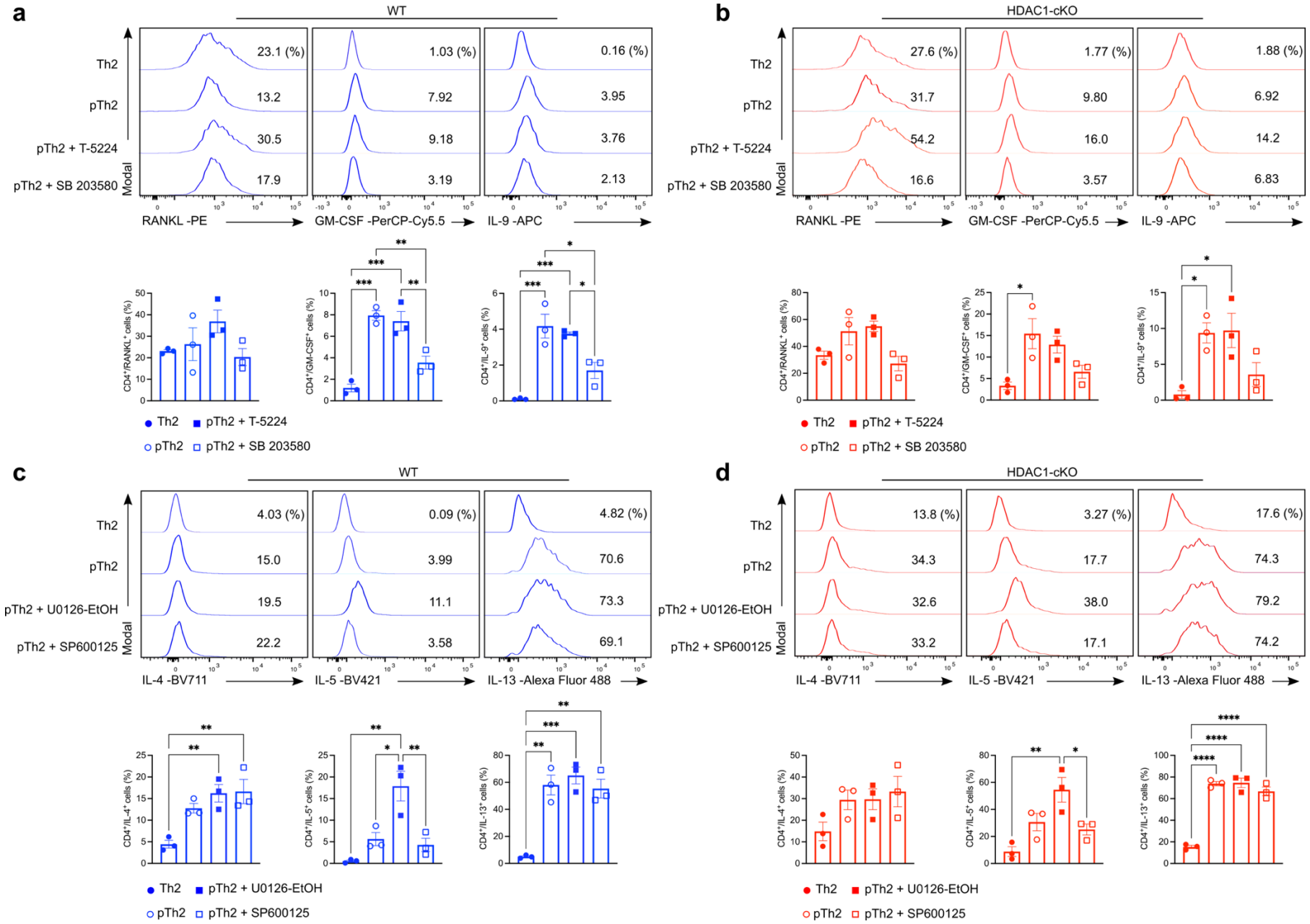

Extended Data Fig.7| Impact of inhibiting AP-1 and MAPKs on *in vitro* generated pTh2 cells. a-d, Targeting p38 MAPK signalling and AP-1 activity in *in vitro* generated pTh2 cells. Naïve $CD4^+$ T cells from WT and HDAC1-cKO mice were differentiated under Th2-promoting conditions (IL-4, IL-2, anti-IFN-γ, and anti-TGF-β) alone, or pTh2-promoting conditions (IL-4, IL-2, TSLP, DTA-1, anti-IFN-γ, and anti-TGF-β) alone, or pTh2 cells treated with an AP-1 inhibitor (T-5224; 10 μM), or pTh2 cells treated with a p38 MAPK inhibitor (SB 203580; 10 μM), and cultured for 5 days. On day 5, cells were restimulated with PMA and ionomycin in the presence of GolgiStop and GolgiPlug for 4 hours and cytokine analyses were performed by flow cytometry. **a,** Histograms show expression (top) and frequencies (bottom) of RANKL, GM-CSF, and IL-9, respectively, in WT cells (blue). **b,** Histograms show expression (top) and frequencies (bottom) of RANKL, GM-CSF, and IL-9, respectively, in HDAC1-cKO cells (red). **c,d,** Inhibition of ERK1/2 and JNK signalling in *in vitro* generated pTh2 cells. Naïve $CD4^+$ T cells from WT and HDAC1-cKO mice were differentiated under Th2-promoting conditions (IL-4, IL-2, anti-IFN-γ, and anti-TGF-β) alone, or pTh2-promoting conditions (IL-4, IL-2, TSLP, DTA-1, anti-IFN-γ, and anti-TGF-β) alone, or pTh2 cells treated with a MEK1/2 inhibitor (U0126-EtOH; 1 μM) which targets ERK1/2 signalling, or pTh2 cells treated with a JNK inhibitor (SP600125; 1 μM), and cultured for 5 days. On day 5, we restimulated the cells with PMA and ionomycin in the presence of GolgiStop and GolgiPlug for 4 hours and performed cytokine analyses by flow cytometry. **a,** Histograms show expression (top) and frequencies (bottom) of IL-4, IL-5, and IL-13, respectively, in WT cells (blue). **b,** Histograms show expression (top) and frequencies (bottom) of IL-4, IL-5, and IL-13, respectively, in HDAC1-cKO cells (red). Data are pooled from three independent experiments and presented as the mean ± SEM. Each symbol represents one mouse. Statistical analysis was performed using a one-way ANOVA with Tukey's multiple comparisons test. $^{*}P<0.05$, $^{**}P<0.01$, $^{***}P<0.001$, $^{****}P<0.0001$. TSLP, thymic stromal lymphopoietin; DTA-1, an agonistic antibody against GITR (TNFRSF18). AP-1, activator protein-1; MAPKs, mitogen-activated protein kinases; p38 MAPK, p38 mitogen-activated protein kinase; ERK, extracellular signal-regulated kinase; JNK, c-Jun N-terminal Kinase.

Extended Data Figure 8